Available online at www.sciencedirect.com

ScienceDirect

Underground Space xxx (2018) xxx–xxx

www.elsevier.com/locate/undsp

Numerical analysis and capacity evaluation of composite sprayed concrete lined tunnels

Alan Bloodworth [a,*], Jiang Su [b]

[a] School of Engineering, University of Warwick, Library Road, Coventry CV4 7AL, UK
[b] Tunnels, AECOM, Croydon, UK

Received 29 June 2017; received in revised form 9 October 2017; accepted 6 December 2017

Abstract

Spray-applied membranes for waterproofing of sprayed concrete tunnels have led to the possibility of shear transfer between primary and secondary linings through the membrane interface, with the potential for reducing overall lining thickness. Laboratory tests have shown a reasonable degree of composite action in beam specimens. In this study, a numerical model previously calibrated against such tests is applied to a whole tunnel, considering soil–structure interaction and staged lining construction. The model shows composite action, and load sharing between the lining layers is expected in the tunnel as in the beams. Parametric studies over the practical range of interface stiffness values show that composite action is maintained, although at high interface stiffness, excessive bending may be imposed on the secondary lining, requiring additional reinforcement. An efficient composite shell design with minimal additional reinforcement is achievable if the secondary lining thickness is reduced as compared to current practice. Robustness of the system, measured in terms of the interface's ability to transfer stress under unequal loading causing distortion on the tunnel, is found to be generally adequate. However, adjacent construction in close proximity may provide insufficient margin on membrane tensile de-bonding, particularly if the membrane is partially or fully saturated.

Keywords: Composite sprayed concrete lining; Spray-applied waterproofing membrane; Interface parameters; Lining efficiency

Introduction

Historically, sprayed concrete lined (SCL) tunnels were usually designed so that the primary lining takes all short-term loads and then degrades to "gray rock" in the long term (Hurt, 2002). The secondary lining was assumed to take all long-term loads, with no load sharing between sacrificial primary and permanent secondary linings.

In the last 20 years, rapid developments from this approach of using a sacrificial primary lining have occurred (Su & Thomas, 2015). Three of these have been (i) incorporation of wet-mix sprayed primary lining as permanent load-bearing structure, (ii) replacement of conventional sheet membrane between primary and secondary linings with double-bonded spray-applied waterproofing membrane, and (iii) use of wet-mix sprayed or cast in situ secondary lining. This configuration is denoted as *composite shell lining* (CSL) and has recently been adopted in soft ground of low permeability (Hasik, Junek, & Zamecnik, 2015; Holter, Bridge, & Tappy, 2010; Nermoen, Grøv, Holter, & Vassenden, 2011; Pickett, 2015). However, SCL tunnels are currently designed generally as *double shell lining* (DSL), a similar configuration to CSL but using an unbonded waterproofing interface with only compressive stiffness, such as with a sheet membrane (Su & Thomas, 2015).

* Corresponding author.
E-mail addresses: a.bloodworth@warwick.ac.uk (A. Bloodworth), Jiang.su@aecom.com (J. Su).

https://doi.org/10.1016/j.undsp.2017.12.001

Please cite this article in press as: Bloodworth, A., & Su, J., Numerical analysis and capacity evaluation of composite sprayed concrete lined tunnels, Underground Space (2018), https://doi.org/10.1016/j.undsp.2017.12.001

However, designing a CSL tunnel as a DSL by ignoring composite action, does not actually achieve an improved lining thickness efficiency, as indicated in Table 1. This refers to three well-known SCL tunnels constructed in London. The first two are the Heathrow Express (Powell, Sigl, & Beveridge, 1997) and Jubilee Line Extension (JLE), London Bridge Station (Dimmock & Lackner, 1998; Zeidler & Gall, 1997) platform tunnels, both built approximately 20 years ago. The third is a typical recently completed Crossrail SCL platform tunnel (Morgan, Wolstenholme, & Dulake, 2013). Although the reinforcement type has progressed from steel mesh and steel reinforcing bars to steel fibers, bringing advantages in health and safety and quality control (Su & Thomas, 2015), the lining efficiency has not changed significantly. This constitutes an urgent need for the industry to understand the mechanical properties of sprayed membrane interfaces, develop appropriate approaches to simulate CSL tunnels, and evaluate their performance with different design parameters under various loading conditions. The first two issues have been investigated by various authors, with their findings discussed in the following section. This study aims to address the third issue.

Technical background and study aims

Recent research (Holter, 2016; Johnson, Swallow, & Psomas, 2016; Nakashima, Hammer, Thewes, Elshafie, & Soga, 2015; Su & Bloodworth, 2016; Vogel et al., 2017) has improved the understanding of interface properties of spray-applied waterproofing membranes, giving confidence that there is a tensile and shear bond and mobilization of a degree of composite action between the primary and secondary linings. However, it is inevitable that key mechanical properties such as interface strength and stiffness will vary over a range due to a number of factors, such as the physical parameters of the interface itself (substrate roughness and membrane thickness), type of spray-applied membrane and the manufacturer, workmanship issues on site (e.g., variation in primary lining and membrane thicknesses), load duration (short-term or long-term), and whether the membrane itself is in the dry state or is partially or fully saturated due to water ingress through cracks in the primary lining. Membrane saturation has been proved to affect water-based ethyl-vinyl-acetate (EVA) polymer-based membranes, reducing their strength in tension and shear (Holter & Geving, 2015).

Therefore, the industry is a long way from obtaining one general set of agreed interface properties (strength and stiffness) to model the sprayed membrane interface under any circumstance. This would require much more experimental data than currently available. It is likely that individual projects will for some time need to commission tests for their chosen membrane material under their own conditions, including representative workmanship and moisture, as the composite shell increasingly becomes the norm for SCL design.

It is understood that there is doubt on the long-term tensile strength of the interface once the material becomes partially or fully saturated. This research anticipates that this issue will be overcome as the body of experimental data grows and/or new or modified membrane materials are developed, and therefore, looks forward to investigating the impact of composite action on the behavior of an actual SCL tunnel and how to exploit it to the fullest. Field monitoring data for SCL tunnels focus mostly on the performance of primary linings (Clayton, Hope, Heymann, Van der Berg, & Bica, 2000; Clayton, Van Der Berg, Heymann, Bica, & Hope, 2002; Clayton, Van Der Berg, & Thomas, 2006; De Battista et al., 2015) and there is a lack of data on load sharing between permanent primary and secondary linings.

Attempts have been made to predict the behavior of composite SCL tunnels using either analytical solutions or numerical modeling (Jager, 2016; Marcher, John, & Ristic, 2011; Pillai, Clement, & Traldi, 2017; Sun, McRae, & Van Greunen, 2013; Thomas & Pickett, 2011), but these have not considered all the key factors of groundwater, different stress states of the primary and secondary linings, soil–structure interaction induced lining deformation, and resulting changes in lining and interface stresses. A numerical modeling methodology capturing all the effects of such factors, leading to a lining capacity evaluation, has not been performed.

This study applies a numerical analysis of a typical tunnel in the ground with lining layers represented as continuum elements with a membrane interface in between, and performs parametric studies to investigate the influence of interface stiffness, reduction of secondary lining thickness relative to that of the primary lining, and unequal loading

Table 1
Lining efficiency progress for SCL tunnels constructed in London.

Platform tunnel lining configuration		Heathrow express/JLE London Bridge Station	Crossrail
Primary lining	Thickness (mm)	300	400
	Type of reinforcement	Steel mesh	Steel fibers
Secondary lining	Thickness (mm)	300	300
	Type of reinforcement	Steel rebars	Steel fibers (steel rebars in the invert)
Tunnel	Total thickness (T) (mm)	600	700
	External diameter (D) (m)	9[a]	11[a]
Lining Efficiency (LE)	T/D (mm/m)	67	64

[a] Approximate values.

Please cite this article in press as: Bloodworth, A., & Su, J., Numerical analysis and capacity evaluation of composite sprayed concrete lined tunnels, Underground Space (2018), https://doi.org/10.1016/j.undsp.2017.12.001

inducing bending in the lining. First, the phenomenon of composite action is defined for this context and the method for evaluating the capacity of a steel fiber-reinforced lining is described.

Membrane interface properties and composite action

Interface normal and shear stiffness values are denoted by *Kn* and *Ks* respectively; they commonly have units of GPa/m and are calculated from measured stiffness values of test specimens loaded in tension/compression and shear respectively, divided by the interface area. Su and Bloodworth (2016) described a program for such tests on samples made with EVA-based membrane interfaces.

The degree of composite action (*DCA*) of a lining with two layers may be quantified by comparing the flexural stiffness of a beam sample manufactured from the lining in question with that of a fully composite beam (i.e., with full continuity between the lining layers) and a non-composite beam (with free sliding between layers).

Thus,

$$DCA = \frac{k_{comp} - k_{non}}{k_{full} - k_{non}} \quad (1)$$

where k_{comp}, k_{non}, and k_{full} are the equivalent flexural stiffness of the composite, non-composite, and fully composite beam respectively for a given loading and support condition. *DCA* ranges between 0.0 (non-composite) and 1.0 (fully composite). k_{comp}, k_{non}, and k_{full} may be derived from deflection data of a suitable flexural test on a beam or panel specimen.

Load effects due to global actions

A CSL normally experiences global combined actions of bending M_{global} and axial force N_{global} (Fig. 1). To evaluate the performance of a component lining layer requires understanding of the load effects induced on it by these global actions. Fig. 2 shows the stress distributions expected due to M_{global} in fully composite, non-composite, and intermediate composite linings, assuming Euler bending. With composite action, M_{global} induces a combination of local bending moment M and local axial force N in each layer, as illustrated in Fig. 3 for the "High" composite case. Furthermore, N_{global} would be divided between the components in proportion to their relative axial stiffness, giving an additional local N to that induced by M_{global}. Hence, N and M in a component lining layer for design depend on both M_{global} and N_{global}. In particular, it is noteworthy that an increased global bending on the lining does not necessarily lead to bending in the individual layers—with high composite action, much of the global bending may be reacted by axial forces.

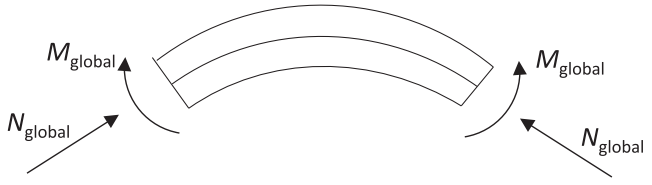

Fig. 1. Global load effects on composite lining.

Capacity and efficiency evaluation

The use of a thrust–moment capacity curve to determine whether a lining has sufficient capacity to sustain the applied load effects was introduced by Sauer, Gall, Bauer, and Dietmaier (1994) and is currently a standard practice. The curve defines the maximum allowable M and N combination for a given concrete cross section (assuming linear elastic-perfectly plastic material behavior), and is a powerful tool for designing primary or secondary linings individually.

Fig. 4 shows an example capacity curve following Eurocode 2 (BSI, 1992) for a 300-mm thick flexural element with 28-day concrete characteristic strength $f_{ck} = 32$ MPa and material partial factor $\gamma_m = 1.5$ (which allows for material variability and reduction in strength and stiffness resulting from material degradation). No contribution from either steel rebar or structural fibers has been included. Excluding both means that where load effects exceed the available capacity, the reinforcement requirements can then be determined. As this study is focused on capacity and robustness, serviceability limit state criteria such as excessive crack width due to tension or bending are not discussed.

The axial force N in an SCL tunnel design is usually limited to below half of its maximum theoretical value when $M = 0$, avoiding brittle concrete crush failure while allowing ductile flexural bending failure to take place in the design space level with or below the tip of the bulge of the capacity curve (Fig. 4). Below the bulge tip, the curve may be approximated as linear, and in Fig. 4, the ratio M/N, which should not be exceeded to avoid additional reinforcement, is 0.13. Example load point 1 with $M/N = 0.05$ is well within the capacity curve, whereas load point 3 with $M/N = 0.20$, which exceeds 0.13, is outside and therefore requires additional steel reinforcement. Thus, obtaining N and M for individual lining layers from a linear-elastic analysis (without partial factor applied to the loads in this study) and examining the ratio M/N is a quick and convenient method of assessing if the lining requires additional reinforcement for a group of tunnels with varying lining thickness and identifying the position around the tunnel that requires additional reinforcement.

It should be noted that the critical ratio M/N is greatest at lower axial force levels (approximately 0.15 as $N \to 0$), reducing as N increases to approximately 0.08 at the bulge tip point, and is also a function of the lining thickness and concrete strength.

As a summary, the criteria for an efficient and robust CSL tunnel design in this study are (i) minimized use of conventional reinforcement, (ii) improved lining efficiency, and (iii) satisfactory robustness of the composite lining

Please cite this article in press as: Bloodworth, A., & Su, J., Numerical analysis and capacity evaluation of composite sprayed concrete lined tunnels, Underground Space (2018), https://doi.org/10.1016/j.undsp.2017.12.001

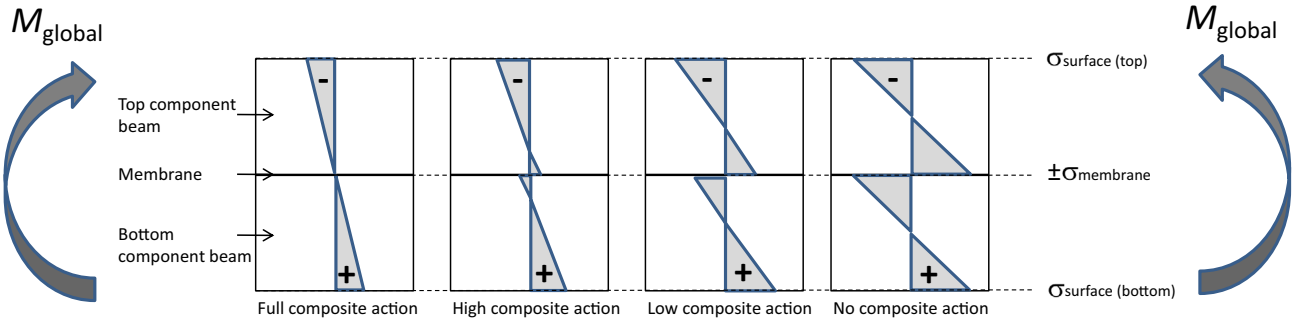

Fig. 2. Composite lining stresses due to global bending.

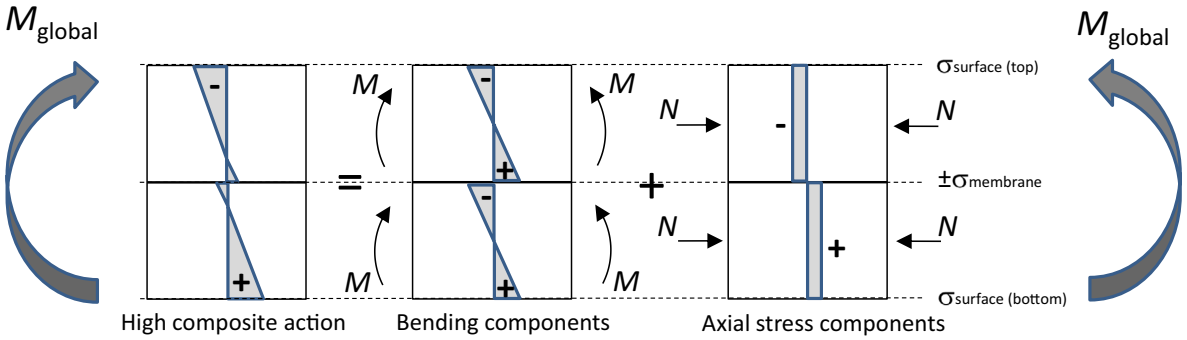

Fig. 3. Breakdown of composite lining stresses due to global bending into bending and axial stress components.

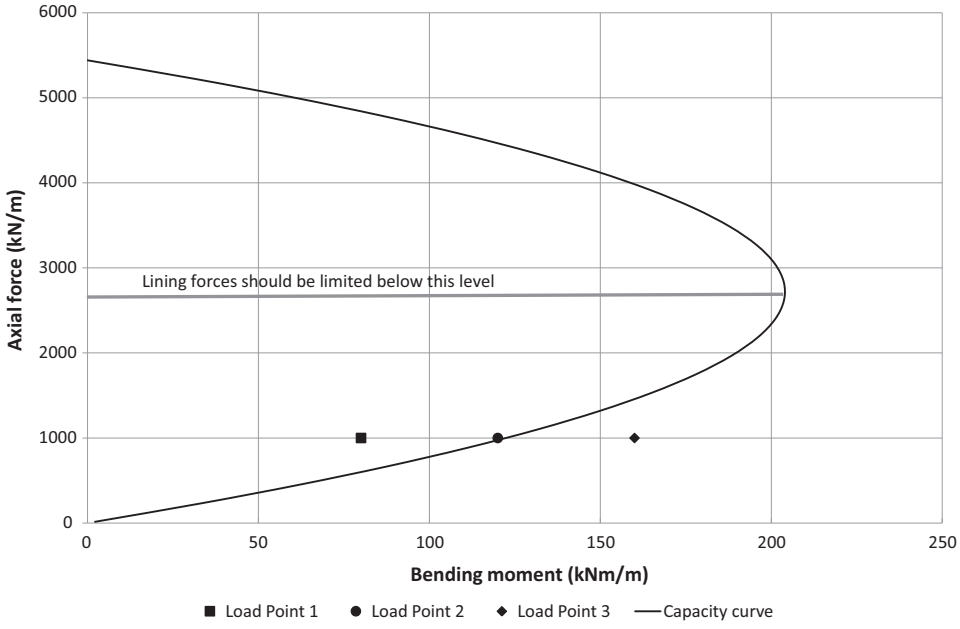

Fig. 4. Capacity curve for 300 mm thick sprayed concrete lining layer.

system (i.e., whether the interface is able to maintain its integrity under realistic external loadings).

Numerical modeling

Numerical modeling is adopted to investigate load sharing between the permanent primary and secondary linings, and concrete–membrane interface stresses, for a typical CSL tunnel in the long term. The approach used was verified in a preceding paper by Su and Bloodworth ("Numerical Calibration of Mechanical Behavior of Composite Shell Tunnel Linings" submitted to Tunneling and Underground Space Technology) against laboratory beam tests with input parameters of *Ks* and *Kn* obtained from element

Please cite this article in press as: Bloodworth, A., & Su, J., Numerical analysis and capacity evaluation of composite sprayed concrete lined tunnels, Underground Space (2018), https://doi.org/10.1016/j.undsp.2017.12.001

tests (Su & Bloodworth, 2016). Parametric studies of beam models in which *Kn* and *Ks* were varied over wide ranges showed that *Ks* had a greater impact than *Kn* on *DCA*, which was maintained between 30% and 80%, indicating that (provided that the membrane strength is sufficient) designers may expect composite action over the practical range of key parameters of the interface (membrane saturation, substrate roughness, membrane type and thickness, etc.).

Although the SCL tunnel excavation is a complex soil–structure interaction problem and 3D modeling is used to understand transient excavation-induced ground deformations and lining forces (Jones, Thomas, Hsu, & Hilar, 2008; Mašín, 2009; Thomas, 2004), because composite action and load-sharing between the lining layers are long-term phenomena and the precise tunnel excavation sequence is not the key focus, this study uses a plane strain 2D analysis. The analysis is performed using the finite difference (FD) FLAC software (Itasca, 2008) by adopting an explicit approach in which, iteration is used to achieve a final converged state. Beam elements are commonly used to represent the primary and secondary linings in an SCL tunnel, but this cannot simulate composite mechanical behavior because beam elements do not have real physical thickness. Instead, in this study, the lining layers are represented as continuum grids of zones with finite physical thickness, and interface elements are employed between the layers with *Kn* and *Ks* assigned.

Model geometry and boundary conditions

The FD grid used for modeling a 10.8 m nominal diameter tunnel with 20 m axis depth is shown in Fig. 5. To represent the soil strata of the London basin, the model consisted of two materials (Table 2). The top and bottom boundaries represent the ground surface and top of Chalk bedrock respectively, with the bottom boundary fixed in both vertical and horizontal directions. The side boundaries were set at a required distance to reliably predict the lining forces and ground deformation around the tunnels, and fixed horizontally. Overground development is simulated as 75 kPa ground surface surcharge.

The ground model comprises 28,500 FD zones, with a fine grid of 25,000 zones (0.2 m × 0.2 m) in the area of high strain gradient around the tunnel and a coarse mesh of 3500 zones in the remainder. Fig. 6 shows the details of the tunnel, including the stages of lining construction and five key locations where results will be analyzed. The lining is modeled with 688 FD zones (equal numbers for primary and secondary linings), with most zones approximately 0.15 m × 0.15 m and slightly larger for the thicker secondary lining invert. Interface elements connect the primary and secondary layers, with properties discussed in section 'Membrane interface properties'.

Ground constitutive model

Geotechnical parameters of the ground were derived from site investigation and laboratory tests for typical London sites (Table 3). The made ground was modeled as linear elastic (constant stiffness with depth). Calibration at Heathrow demonstrated that London Clay is best represented by an anisotropic soil model with higher horizontal stiffness (Chang, Scott, & Pound, 2001; Scott, Pound, & Shanghavi, 2003). However, anisotropy is not expected to significantly affect the long-term load sharing between the primary and secondary linings and therefore, an isotropic elastic-perfectly plastic model was adopted, with stiffness as the average of the horizontal and vertical values. Nonlinear stiffness of London Clay was simulated by the Jardine A* function (Eadington & O'Brien, 2011; O'Brien & Harris, 2013) with parameters given in Table 4, where z is the depth below the top of London Clay. Tresca theory is used to model the soil shear strength. Short-term (prior to and during construction) and long-term pore water pressure profiles are the same, with groundwater taken at the top of London Clay and pore pressure increasing linearly at a rate of 70% of the hydrostatic pressure.

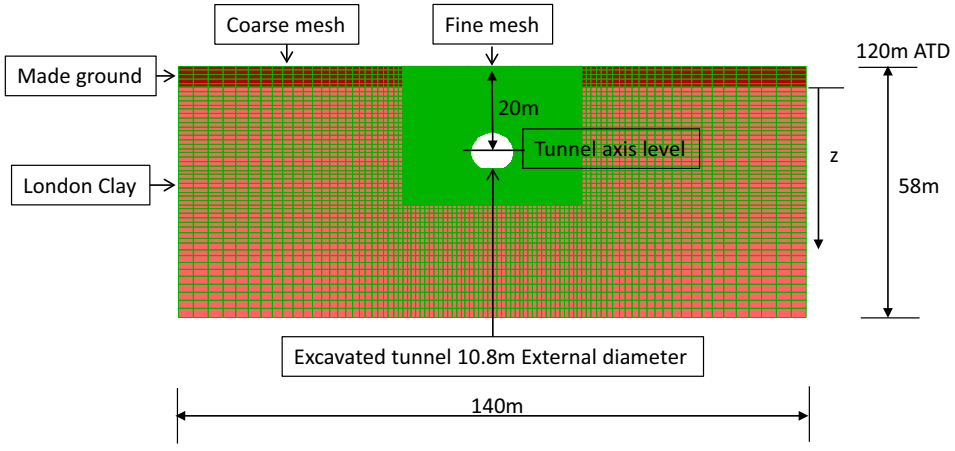

Fig. 5. Complete finite difference grid.

Please cite this article in press as: Bloodworth, A., & Su, J., Numerical analysis and capacity evaluation of composite sprayed concrete lined tunnels, Underground Space (2018), https://doi.org/10.1016/j.undsp.2017.12.001

Table 2
Geological stratigraphy.

Depth from [mATD]	Base [mATD]	Thickness [m]	Description
120.00	113.00	7.00	Made Ground (MG)
113.00	62.00	51.00	Upper London Clay (ULC) – unit B/A3

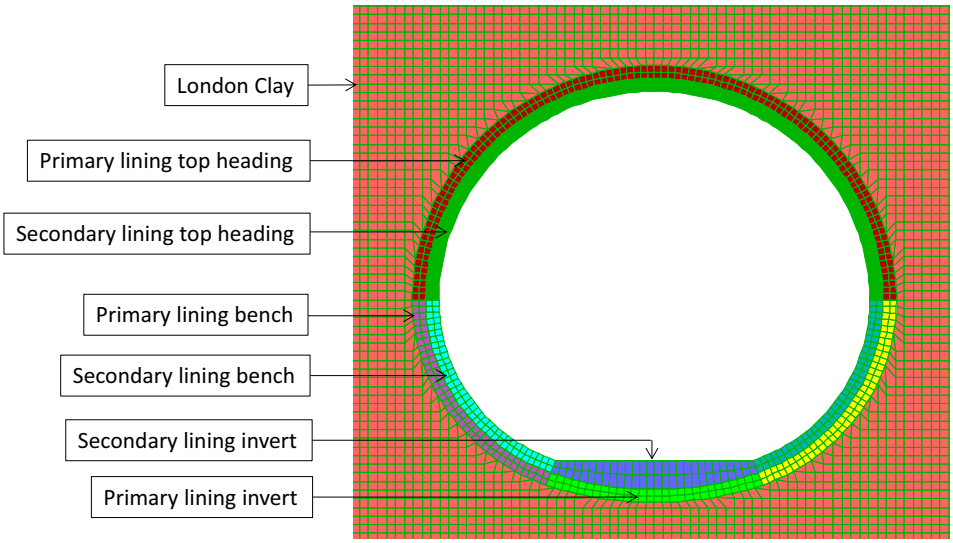

Fig. 6. Detail of finite difference model at tunnel.

Table 3
Geotechnical ground parameters.

Soil stratum	Made ground	Upper London clay
Bulk unit weight [kN·m^{-3}]	20	20
Coefficient of earth pressure at rest K_0	0.5	1.2
Undrained shear strength c_u [kPa]	-	$70 + 11z$
Effective cohesion c' [kPa]	0	10
Effective friction angle ϕ' [deg]	25	20
Porosity n [%]	35	45
Drained Poisson's ratio ν'	0.3	0.1
Drained elastic modulus E' [kPa]	5000	ε_s and p' dependent using Jardine function

Tunnel model

The lining geometry is shown in Fig. 7. All dimensions are extrados to extrados. Lining layers are each 300-mm thick, except where the secondary is thickened to 650 mm in the invert. Excavation is performed first by a 5.3 m diameter circular pilot tunnel, with enlargements in three steps: top heading (TH), bench (BCH), and invert (INV). Joints between stages of the primary lining are rigidly connected, with full force and moment transfer (using the FLAC command "attach"). Low stiffness beam elements attached at mid-depth of each lining layer provide the output of axial force and bending moment, as verified by Su (2015). Discontinuities in load effects are anticipated at joints between primary lining stages, because beam elements cannot be used in zones where "attach" is also used.

The 28-day concrete characteristic strength is 32 MPa. The J2 curve (Osterreichischer Betonverein, 1999) is used for development of strength under immediate loading up to 4 h, followed by the Chang and Stille (1993) equation for the period of up to 28 days (dotted line in Fig. 8), after which the strength is assumed constant. The development of stiffness also follows the method by Chang and Stille (1993). A corresponding curve for long-term loading (Fig. 8) is derived by adopting a creep factor of 2.0.

In the analysis, the tunnel construction sequence (after the pilot tunnel) was (1) two top headings, (2) double bench, and (3) double invert. Construction of each top heading was assumed to take 12 h, while the double bench and double invert 6 h each. Sprayed concrete stiffness was calculated according to its age when the next construction step starts. For example, the age of the crown lining is 24 h

Table 4
Jardine A* parameters for upper London Clay.

A*hh0 [kPa]	A	B	C	α	γ	ε_{amin}	ε_{amax}	G_{min} [kPa]
5500+60z	0.43	0.27	5.0×10^{-5}	1.76	0.81	5.0×10^{-5}	2.0×10^{-3}	6000

Please cite this article in press as: Bloodworth, A., & Su, J., Numerical analysis and capacity evaluation of composite sprayed concrete lined tunnels, Underground Space (2018), https://doi.org/10.1016/j.undsp.2017.12.001

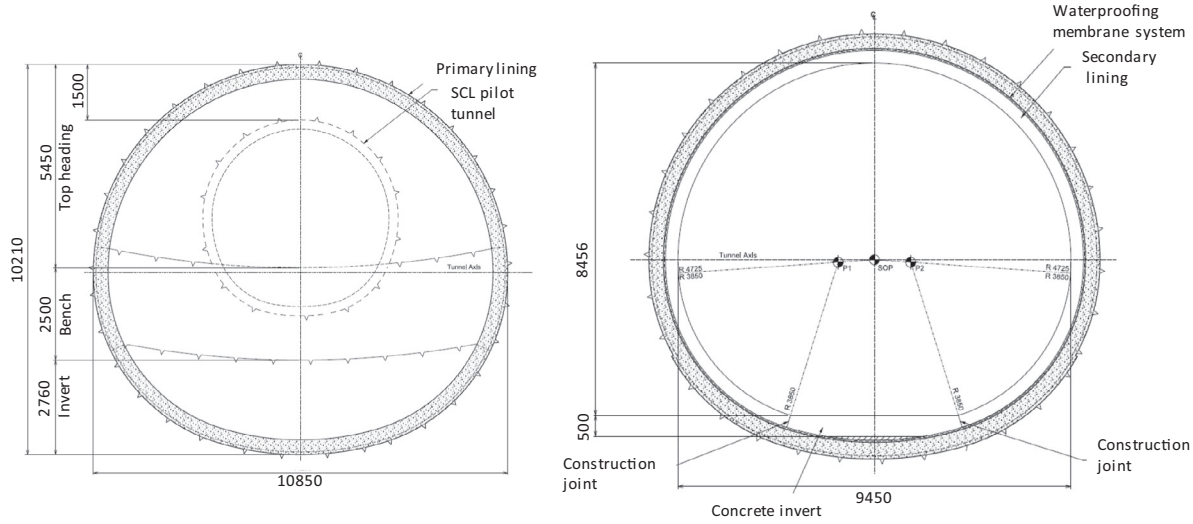

Fig. 7. SCL tunnel primary and secondary lining geometry.

at completion of the top headings, 30 h following double bench excavation, and 36 h at ring closure.

Membrane interface properties

The interface is modeled as linear elastic-perfectly plastic with tensile and shear strengths of 0.8 MPa and 2.0 MPa respectively—both minimum values that are obtained from laboratory tests on "dry" specimens (Su & Bloodworth, 2016).

In the verification of the numerical modeling approach described herein against laboratory beam tests by Su and Bloodworth ("Numerical Calibration of Mechanical Behavior of Composite Shell Tunnel Linings" submitted to Tunneling and Underground Space Technology), base case stiffness values $Kn = 8$ GPa/m and $Ks = 4$ GPa/m were selected as representative of a "dry" interface formed with as-sprayed primary lining and relatively thin membrane (the most likely practical interface combination) under immediate loading. These were further proposed to be halved for long-term loading (Su & Bloodworth, 2016) to $Kn = 4$ GPa/m and $Ks = 2$ GPa/m, for which the beam model predicted a DCA of 0.56. These long-term values become the base case values for analysis in this study.

Tunnel construction process

Construction-induced short-term ground deformation and lining forces were simulated using the stress reduction method (Panet & Guenot, 1982), which assumes a fictitious tunnel internal pressure first set to the initial ground stress and then reduced by a certain percentage to model

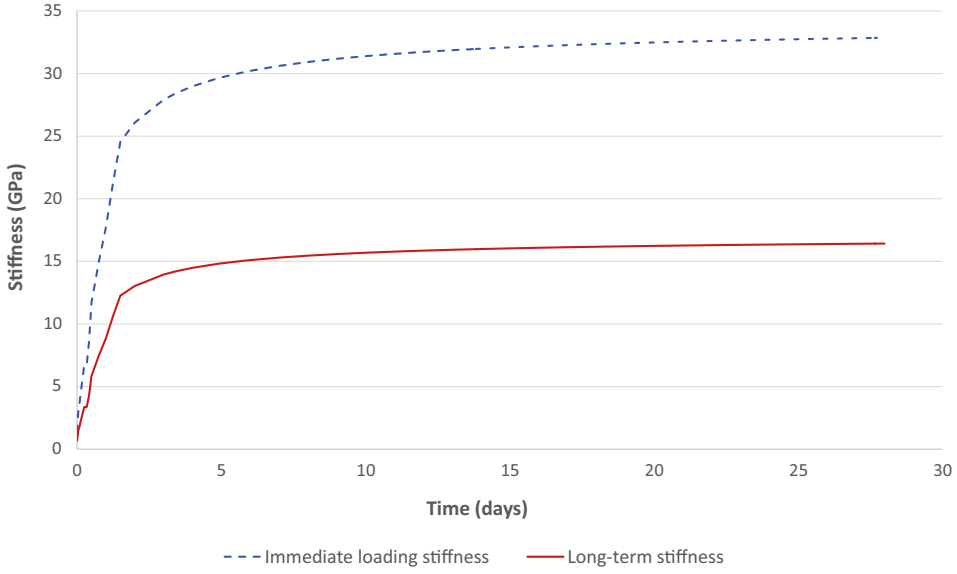

Fig. 8. Sprayed concrete early age stiffness development.

Please cite this article in press as: Bloodworth, A., & Su, J., Numerical analysis and capacity evaluation of composite sprayed concrete lined tunnels, Underground Space (2018), https://doi.org/10.1016/j.undsp.2017.12.001

sequential tunnel excavation, allowing the lining to deform and carry a proportion of the initial ground stress. Stress relaxation ratios have been calibrated against monitoring data for previous SCL tunnel construction in London (Mott MacDonald, Heathrow Express SCL Tunnel – Calibration Report for Relaxation Methodology. Unpublished report) and are presented in Table 5. As an example, when the pilot tunnel face is excavated but before the lining is installed, the tunnel internal pressure is reduced from 100% to 50% of the initial ground stress. A graphical representation of the stages indicated in Table 5 is shown in Fig. S1 in the Supplemental data.

In the short term, the ground is assumed to behave as undrained, and the lining modeled as impermeable. Assuming that the tension bond strength of the waterproofing membrane interface is not exceeded, there is no difference between applying a long-term water pressure to the extrados of the primary lining or the extrados of the waterproofing membrane interface. After excavation of the ground and installation of the primary lining at each construction stage, an undrained equilibrium of loads in the ground and tunnel lining is obtained. Then interface elements and secondary lining zones are installed in one step and assigned their long-term properties to model the 120-year design life. Drained equilibrium is executed and Mohr–Coulomb theory is used to model the soil shear strength.

The loading speed is automatically set by the program according to the stiffness of the structures in the model. The convergence criterion used in FLAC is the maximum unbalanced force ratio, which is a ratio between the algebraic sum and the mean absolute value of forces acting on a grid point from its neighboring elements. A system is usually considered in equilibrium when this ratio is sufficiently small, and for this study, it was taken as less than 10^{-5}.

Base case analysis

The first analysis was carried out with the aforementioned base case stiffness values $Kn = 4$ GPa/m and $Ks = 2$ GPa/m assigned to the interface around the whole tunnel.

Fig. 9 shows the primary lining axial force and bending moments at the end of construction of the primary lining. The axial force gradually increases from 850 kN at the crown to approximately 1100 kN at the axis, before reducing to approximately 450 kN at the invert. The lining at the top heading, being the first part to be built, accumulates more axial force compared to the bottom half. The greatest bending moment occurs between the axis and knee, attributed to the increased lining curvature due to the flattened tunnel profile (Fig. 7).

Load sharing is evaluated by how long-term consolidation load effects, i.e., changes in load effects in the primary and secondary linings between the short and long-term stages, are shared. Fig. 10 shows the consolidation axial force and bending moment for the primary and secondary lining components. The primary lining carries more axial force above the shoulder and below the knee but less between the shoulder and the knee. A 50 kN of pure tension occurs at the secondary lining crown due to the mode of tunnel deformation, as will be discussed later. The secondary lining carries more bending moment at all positions except the knee, due to the complex ground–structure interaction and composite action between the primary and secondary linings, as will be discussed further in the following sections.

Fig. 11 shows the lower portion of the lining capacity curve of Fig. 1, indicating the plotted points representing the load effects in the primary and secondary linings. Primary lining effects are well within the capacity curve while some secondary lining effects are outside. Primary lining axial forces of 1000–1200 kN are well below the 50% axial force capacity line in Fig. 4. This is typical because lining forces are not factored and spare primary lining capacity is usually maintained to resist loading from compensation grouting and construction of adjacent underground structures.

Plotting the M/N ratio around the tunnel is used to identify locations in the secondary lining with insufficient capacity (Fig. 12). M/N above the shoulder and below the knee is either greater than 0.13 (causing bending failure) or less than zero (tension failure), which means that reinforcement is required at these two areas.

Fig. 13 shows the normal and shear interface stresses. The maximum normal interface stress is approximately 20 kPa compression at the crown, changing almost linearly to the maximum tension of approximately −150 kPa at the axis. It then reduces to approximately zero at the construction joints between the knee and invert, before increasing back to −70 kPa (tension) at the center of the invert, which is well below the tension limit of 0.8 MPa.

Table 5
Stress relaxation ratios.

Tunnel	Stage	TH	BCH	INV
SCL pilot tunnel	Full face excavation	100–50%		
	Lining installation	50–0%		
SCL tunnel enlargement	Enlarge whole tunnel	100–75%	100	100–75%
	Install TH lining	75–50%	100–75%	75–50%
	Install BCH lining	50–25%	75–50%	50–25%
	Install INV lining	25–0%	50–0%	25–0%

Please cite this article in press as: Bloodworth, A., & Su, J., Numerical analysis and capacity evaluation of composite sprayed concrete lined tunnels, Underground Space (2018), https://doi.org/10.1016/j.undsp.2017.12.001

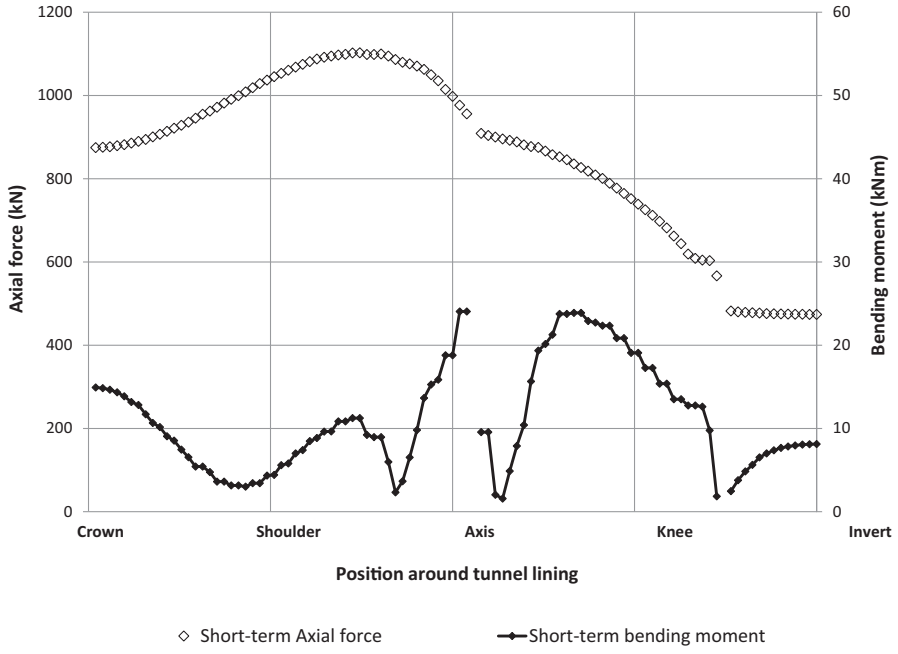

Fig. 9. Primary lining short-term axial force and bending moment.

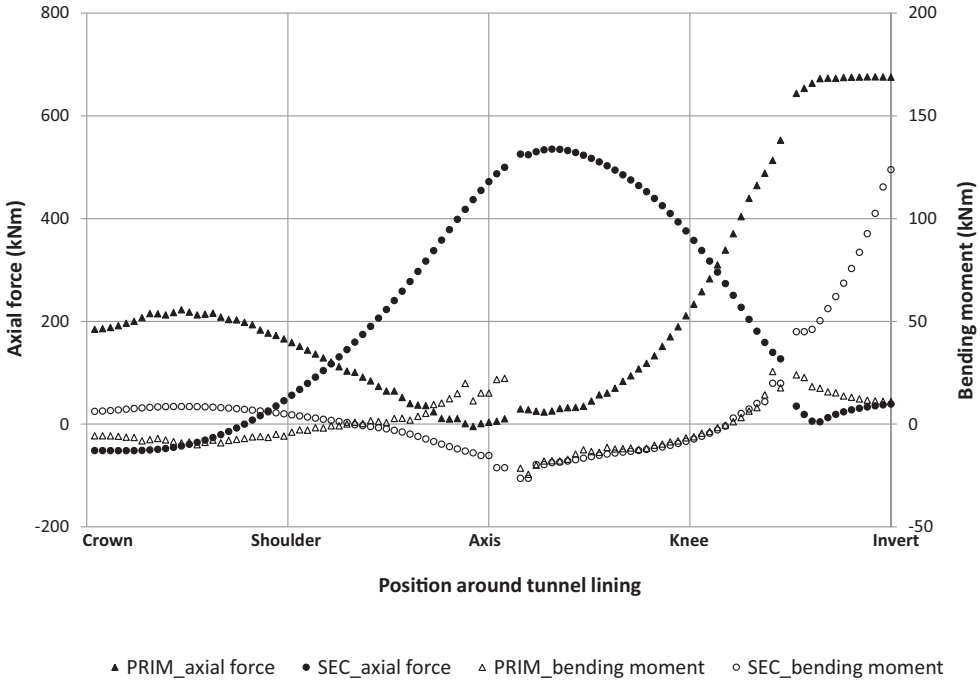

Fig. 10. Long-term consolidation axial force and bending moment for the primary and secondary linings.

Tensile interface stresses at the axis indicate that the secondary lining has been stretched horizontally outward, pulling the crown into tension. The interface at the invert is in tension because the higher bending moment in the secondary lining induces a greater deformation than in the primary lining. These are consistent with the lining deformations shown in the vector plot of displacements in Fig. 14 (at exaggerated scale), in which the circle represents the original tunnel profile.

The shear interface stress varies between 0 and 135 kPa from the crown to the axis and changes to −170 kPa (opposite direction) at the knee, before returning to zero at the center of the invert. These are all well below the shear stress limit of 2 MPa. The highest shear interface stresses

Please cite this article in press as: Bloodworth, A., & Su, J., Numerical analysis and capacity evaluation of composite sprayed concrete lined tunnels, Underground Space (2018), https://doi.org/10.1016/j.undsp.2017.12.001

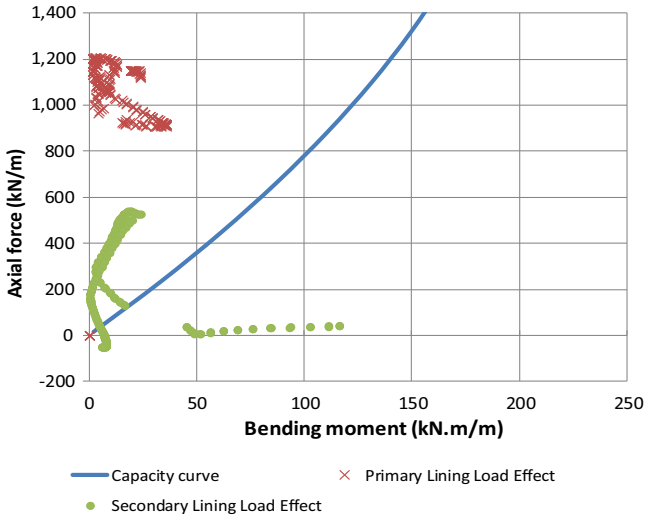

Fig. 11. Capacity curve and primary and secondary lining component load effects.

(i.e., the highest bending curvatures) occur at the shoulder and knee, consistent with the lining deformations shown in Fig. 14.

Figs. 15 and 16 compare the axial forces and bending moments respectively of the base case CSL with that of fully composite and non-composite (i.e., double shell) tunnels of the same dimensions, ground conditions, and construction sequence, to demonstrate the impact of composite action. It can be observed that the axial forces and bending moments of the base case are close to those of the fully composite lining.

Interface parametric studies

Following the base case investigation, three series of parametric studies were carried out. The first investigates the impact of variance in *Kn* and *Ks*, considering their impact first individually and then when varied simultaneously over a design space exceeding the practical range of *DCA* that originated from experimental tests. The second series investigates whether an improved lining efficiency can be achieved for CSL tunnels, and what its impact might be on reinforcement requirements by varying the secondary lining thickness with the primary held constant. The third series examines the robustness of the CSL tunnel, particularly the interface, to external impacts causing the tunnel lining to distort, modeled in terms of nearby excavation causing stress relief on one side or beneath the tunnel.

In each study, the long-term lining load effects (axial force and bending moment), evaluation of lining capacity, and interface stresses are presented, specifically addressing the need for additional reinforcement, and likelihood of tensile de-bonding or slippage in the interface.

Variation of interface stiffness values Kn and Ks

To reflect a practical interface stiffness variation due to different manufacturers' products, variance of workmanship, and effect of membrane partial or full saturation as discussed in the Introduction, *Kn* and *Ks* were multiplied by 10, 100, 0.1, and 0.01 times the long-term base values of 4 GPa/m and 2 GPa/m respectively.

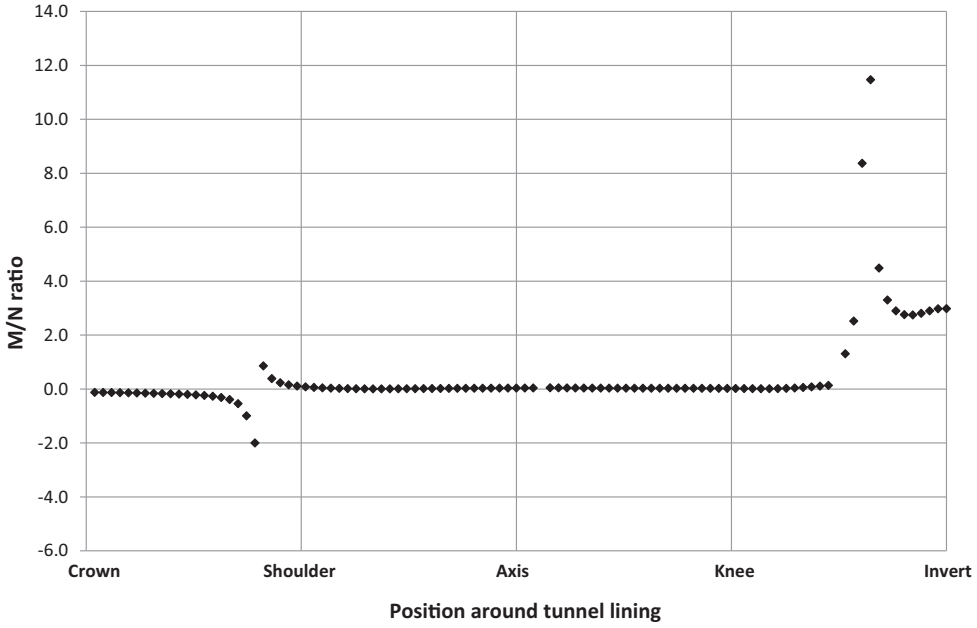

Fig. 12. M/N ratio for secondary lining as a function of position around tunnel.

Please cite this article in press as: Bloodworth, A., & Su, J., Numerical analysis and capacity evaluation of composite sprayed concrete lined tunnels, Underground Space (2018), https://doi.org/10.1016/j.undsp.2017.12.001

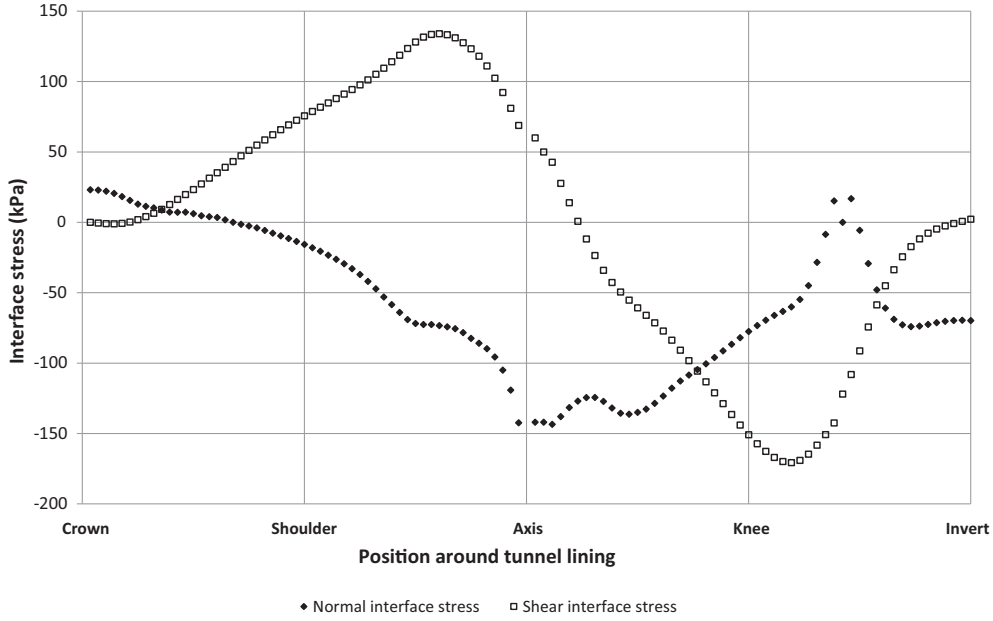

Fig. 13. Normal and shear interface stresses as a function of position around tunnel.

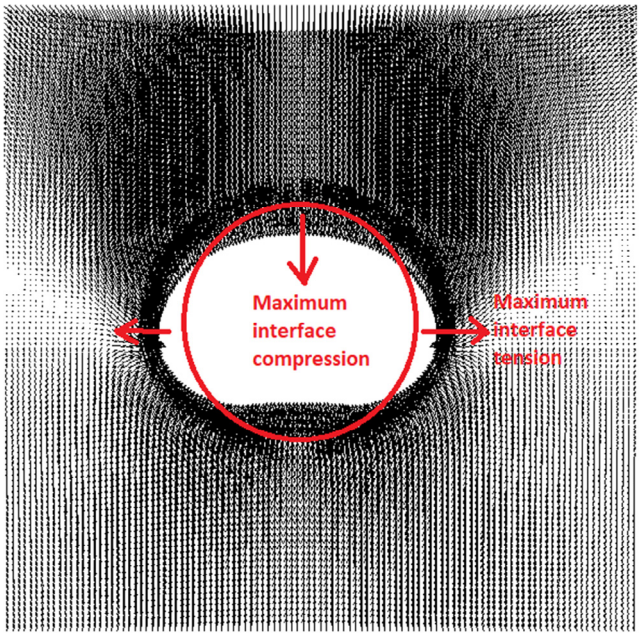

Fig. 14. Deformation of a CSL tunnel.

Interface normal stiffness Kn

Fig. 17(a) and (b) shows that the long-term primary lining axial force decreases and the secondary lining axial force increases with increasing *Kn* up to the base value, at all positions except the crown and invert. This indicates a trend of more consolidation loads being taken by the secondary lining. At the base value *Kn*, the primary lining has transferred all possible force to the secondary lining, mostly due to tunnel lining deformation, and a further increase in *Kn* does not increase the transferred lining forces. This was also observed in the verification analyses on composite beams. Specifically, data for $Kn = 10 \times$ base and $Kn = 100 \times$ base are superimposed. This is proved to be generally true, and therefore, the $Kn = 10 \times$ base case will not be shown in future plots.

The greatest axial force transfer occurs at the axis level. It is noteworthy that for the lowest value of *Kn* (0.04 GPa/m), no tension occurs at the secondary lining crown and less compression is experienced at the axis, because the low interface stiffness allows the secondary lining to deform more freely, reducing the "stretching" effect at the crown.

Fig. 18 shows that as *Kn* is increased up to the base value, the long-term bending moments decrease slightly in the primary lining and increase slightly in the secondary invert, decreasing elsewhere. Again, there is no perceptible change for *Kn* above the base value.

Evaluation of lining capacity

Adequacy of the primary lining as demonstrated for the base case is not a concern as *Kn* is varied—all *M*/*N* ratios are safe. By contrast, Fig. 19 shows that for the secondary lining in all cases, the safety *M*/*N* ratio is exceeded above the shoulder and below the knee. The lower the value of *Kn*, the lower the *M*/*N* ratio, with the exception of $Kn =$ 0.04 GPa/m, for which the secondary lining axial force is much lower than in the other cases, although, the bending moment is similar to that for $Kn = 0.4$ GPa/m, leading to an increase in *M*/*N* ratio.

Interface stresses

Figs. 20 and 21 shows that the normal and shear interface stresses significantly increase in magnitude when *Kn* is increased from 0.04 GPa/m to 0.4 GPa/m but only slightly thereafter. This corresponds with previous observations on the axial force and bending moment. The

Please cite this article in press as: Bloodworth, A., & Su, J., Numerical analysis and capacity evaluation of composite sprayed concrete lined tunnels, Underground Space (2018), https://doi.org/10.1016/j.undsp.2017.12.001

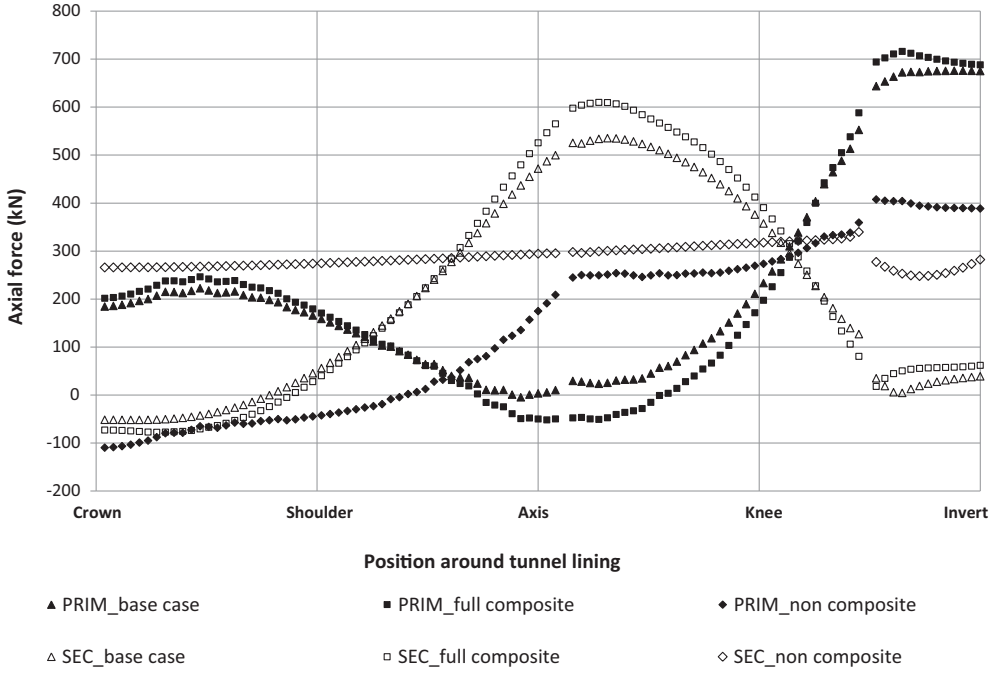

Fig. 15. Comparison of long-term axial forces of base case with non-composite and fully-composite linings.

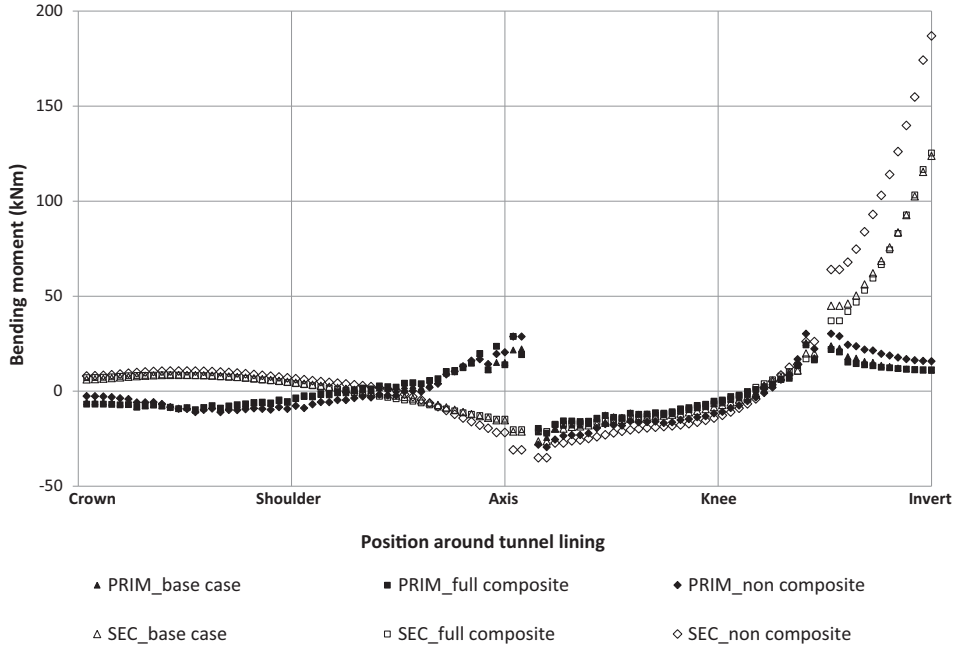

Fig. 16. Comparison of long-term bending moments of base case with non-composite and fully composite linings.

maximum normal and shear interface stresses are 73 kPa (compression), 150 kPa (tension), and 170 kPa (shear) respectively, which are all well within the interface stress limits.

Shear interface stiffness Ks

The trend of the axial force in Fig. 22 is very similar to that in Fig. 17, with the highest secondary lining axial compression occurring at the axis. The higher the *Ks* value, the lower the compression axial force observed at the secondary lining crown. This is because the higher the composite action, the more the global bending is reacted as local axial forces in the two linings. This adds axial tension to the secondary lining at the crown due to the tunnel deformation pattern (Fig. 14), reducing its compression and even causing net tension. For the same reason, the trend of the bending moment in Fig. 23 is very similar to that in Fig. 18 in that the higher the *Ks* value, the lower

Please cite this article in press as: Bloodworth, A., & Su, J., Numerical analysis and capacity evaluation of composite sprayed concrete lined tunnels, Underground Space (2018), https://doi.org/10.1016/j.undsp.2017.12.001

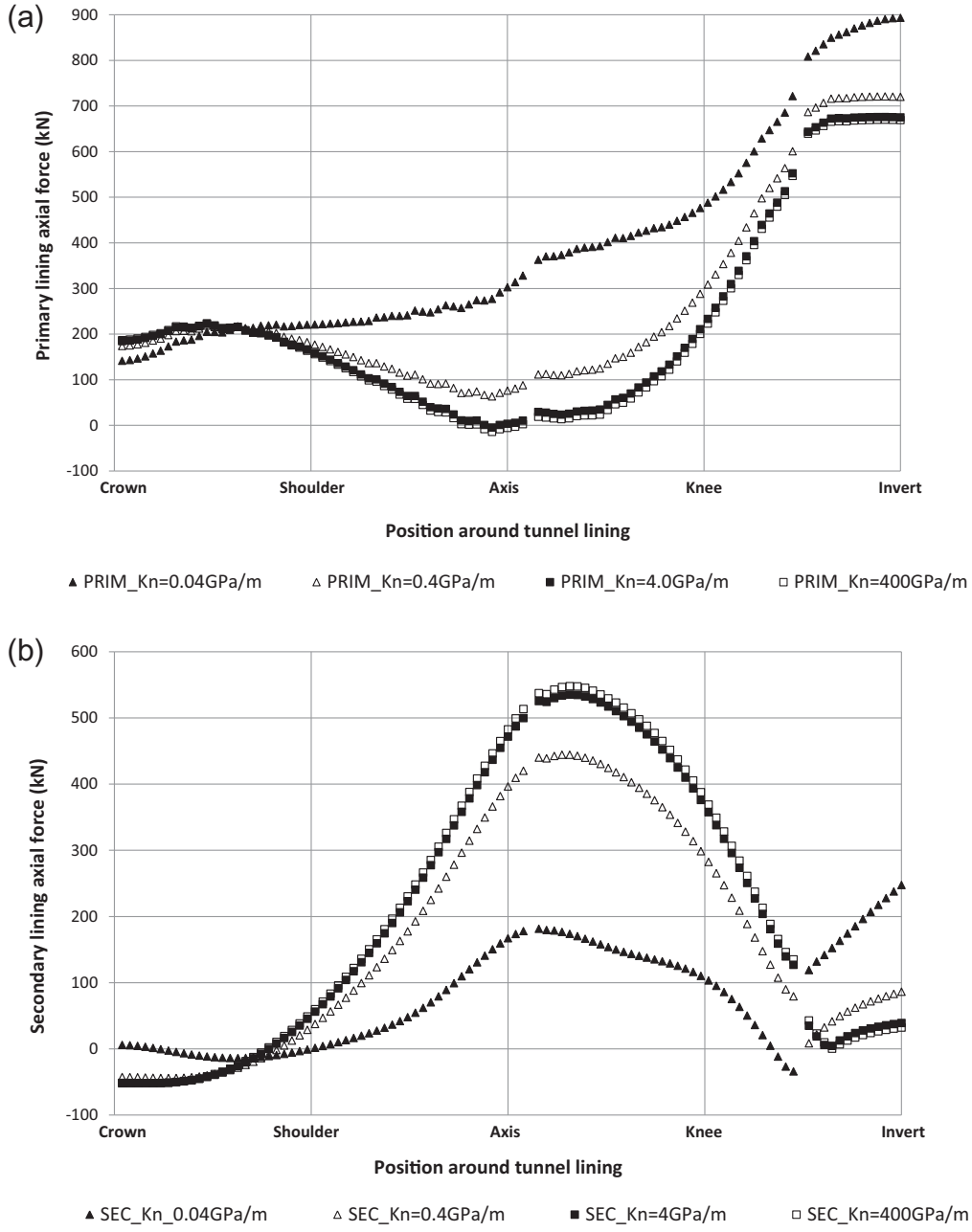

Fig. 17. (a) Sensitivity of primary lining axial force to interface normal stiffness Kn (Ks = 2 GPa/m). (b) Sensitivity of secondary lining axial force to interface normal stiffness Kn (Ks = 2 GPa/m).

the magnitude (i.e., closer to zero) of the bending moment in the primary and secondary linings.

Fig. 24 shows that for the secondary lining in all cases, the safe M/N ratio of 0.13 is exceeded above the shoulder and below the knee, as observed in the study on *Kn*. The lower the *Ks* value, the safer the secondary lining, except for $Ks = 0.02$ GPa/m, as discussed previously.

Plots of the normal and shear interface stresses as *Ks* varies (Figs. S2 and S3 in the Supplemental data) are observed to be very similar to those for *Kn* (Figs. 20 and 21). Interface stresses increase significantly with *Ks* from 0.02 GPa/m to 2 GPa/m, but only slightly thereafter. The maximum interface stresses are 30 kPa (compression), 160 kPa (tension), and 220 kPa (shear), which are all well within the stress limits.

Simultaneous variation of Kn and Ks

Kn and *Ks* were varied simultaneously over the same range of 0.01–100 times the base case values. The results are summarized here, while the plots are available in the Supplemental data (Figs. S4–S9).

For the axial force, the results confirm previous observations that (1) the higher the normal and shear interface stiffness, the greater the proportion of load transferred

Please cite this article in press as: Bloodworth, A., & Su, J., Numerical analysis and capacity evaluation of composite sprayed concrete lined tunnels, Underground Space (2018), https://doi.org/10.1016/j.undsp.2017.12.001

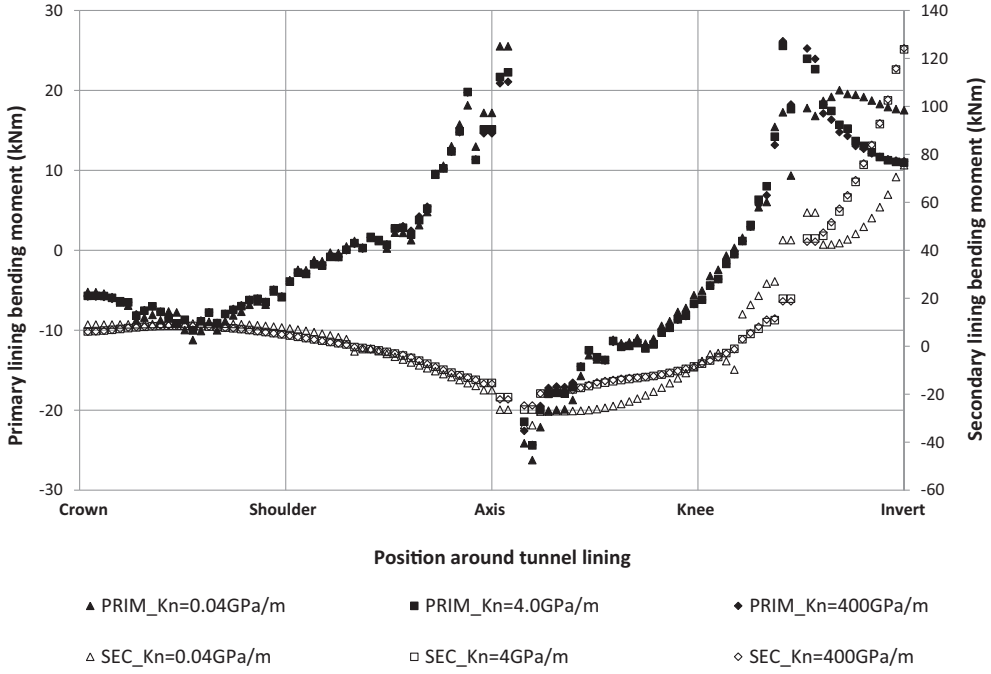

Fig. 18. Sensitivity of primary and secondary lining bending moment to interface normal stiffness Kn (Ks = 2 GPa/m).

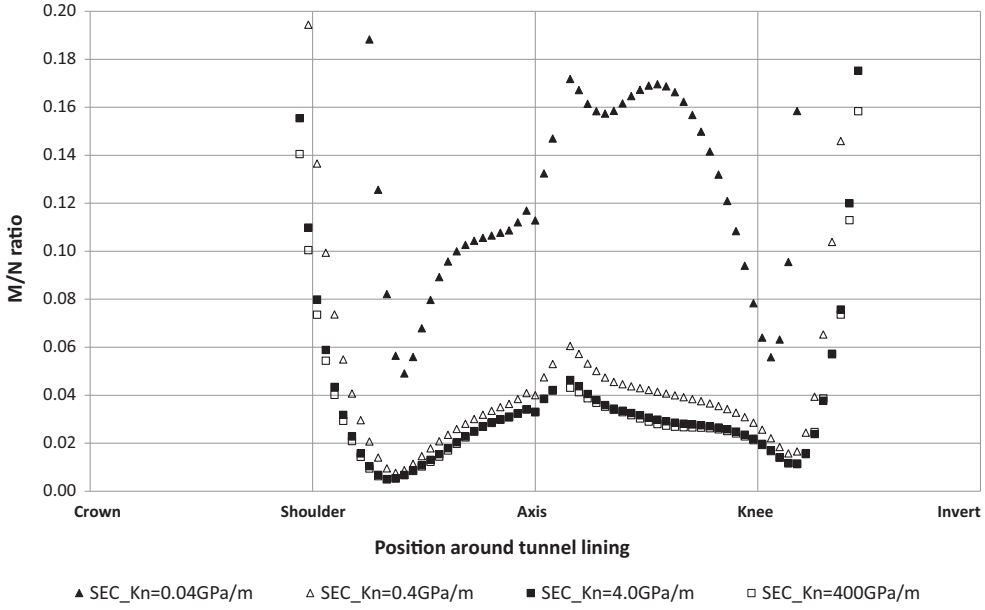

Fig. 19. Sensitivity of M/N ratio for secondary lining to interface normal stiffness Kn (Ks = 2 GPa/m).

from the primary to secondary lining, (2) tension occurs at the secondary lining crown when *Kn* and *Ks* are greater than or equal to base values, and (3) there is little change in axial force with further increase in *Kn* and *Ks* above the base values. For the bending moment, the results also confirm that (1) the higher the normal and shear interface stiffness, the lower the bending moments for both primary and secondary linings, (2) change in bending moments is more rapid for *Kn* and *Ks* reducing below base values than for them increasing above base values.

The primary lining is shown to be safe in terms of *M*/*N* ratio for all cases, while the secondary lining is safe only between the shoulder and knee, as previously observed. The maximum normal and shear interface stresses are very close to the values in the *Ks* sensitivity study and all are within acceptable limits.

Please cite this article in press as: Bloodworth, A., & Su, J., Numerical analysis and capacity evaluation of composite sprayed concrete lined tunnels, Underground Space (2018), https://doi.org/10.1016/j.undsp.2017.12.001

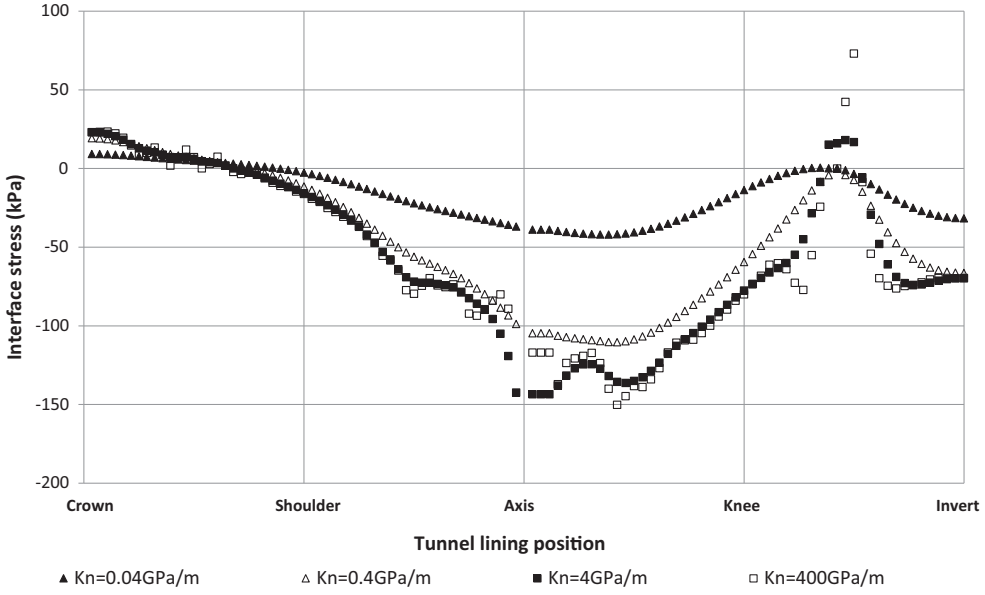

Fig. 20. Sensitivity of interface normal stress to interface normal stiffness Kn (compression positive, Ks = 2 GPa/m).

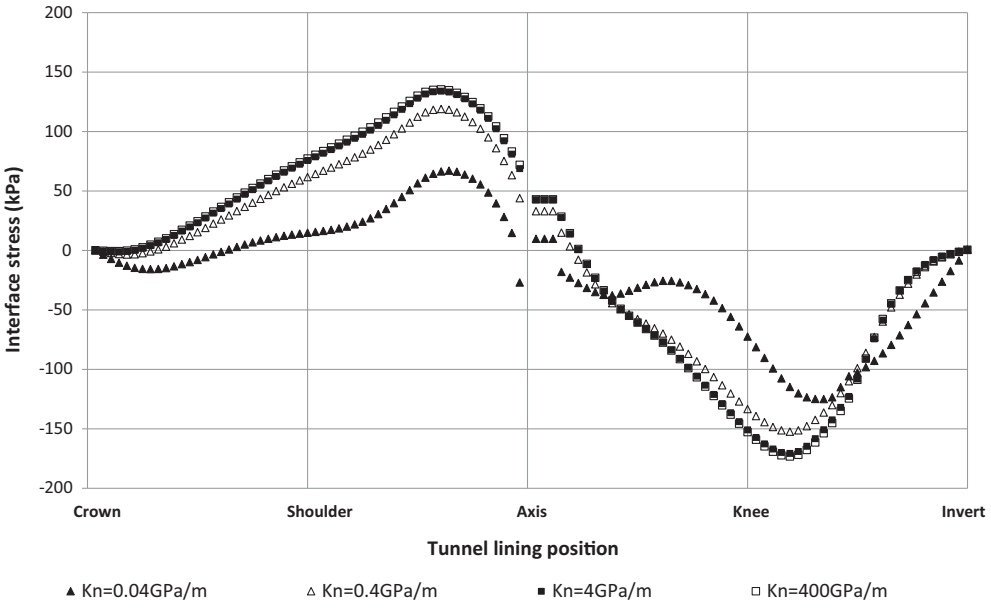

Fig. 21. Sensitivity of shear interface stress to normal interface stiffness Kn (Ks = 2 GPa/m).

Variation in lining thickness

The secondary lining thickness S is varied from 300 mm to 50 mm at 50 mm intervals with the primary thickness P maintained at 300 mm, so that P/S ranges from 1 to 6. M/N ratios and interface stress results are presented and discussed. Base case interface stiffness values are used. Raw results for axial force and bending moment are available in the Supplemental data (Figs. S10–S13).

Fig. 25 shows the sensitivity of primary lining M/N ratio to varying P/S ratio. In all cases, the entire primary lining ring is safe ($M/N < 0.13$). The greater the P/S ratio, the "safer" the primary lining, which is mostly attributed to the faster increase in axial force than in bending moment.

Fig. 26 shows the sensitivity of secondary lining M/N ratio to varying P/S. To confirm the safety of the secondary lining requires first the determination of safe M/N ratios for lining thicknesses below 300 mm, because Fig. 4 is only valid for 300 mm layers. The required values are presented in Table 6 (full capacity curves are given in Fig. S14 in the Supplemental data).

The main observation from Fig. 26 is that as P/S increases (i.e., secondary thickness reduces), M/N reduces around the whole tunnel. However, the safe M/N ratio

Please cite this article in press as: Bloodworth, A., & Su, J., Numerical analysis and capacity evaluation of composite sprayed concrete lined tunnels, Underground Space (2018), https://doi.org/10.1016/j.undsp.2017.12.001

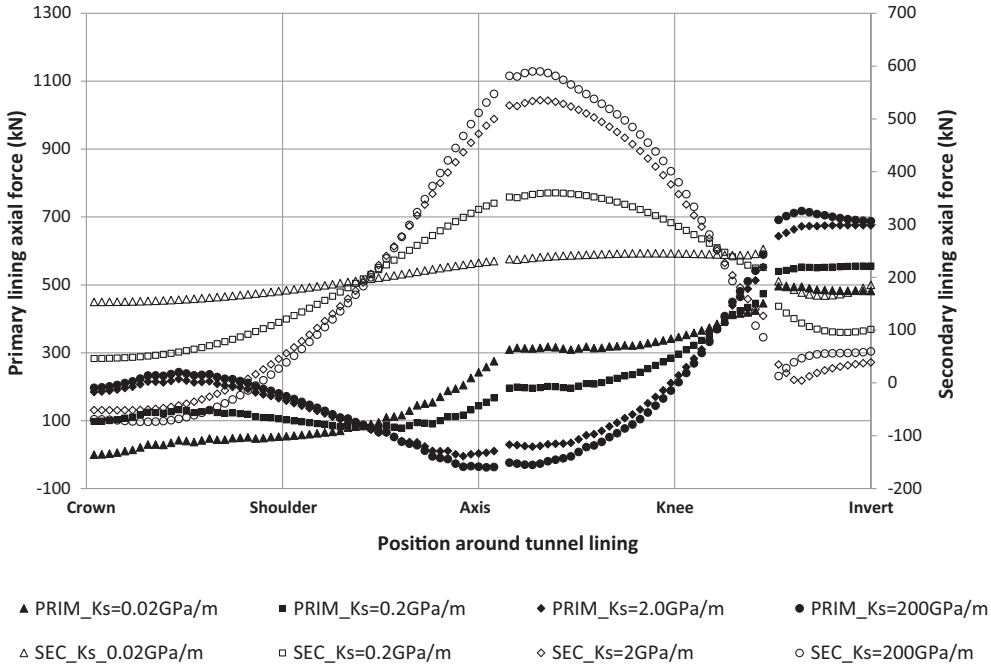

Fig. 22. Sensitivity of primary and secondary lining axial force to shear interface stiffness Ks (Kn = 4 GPa/m).

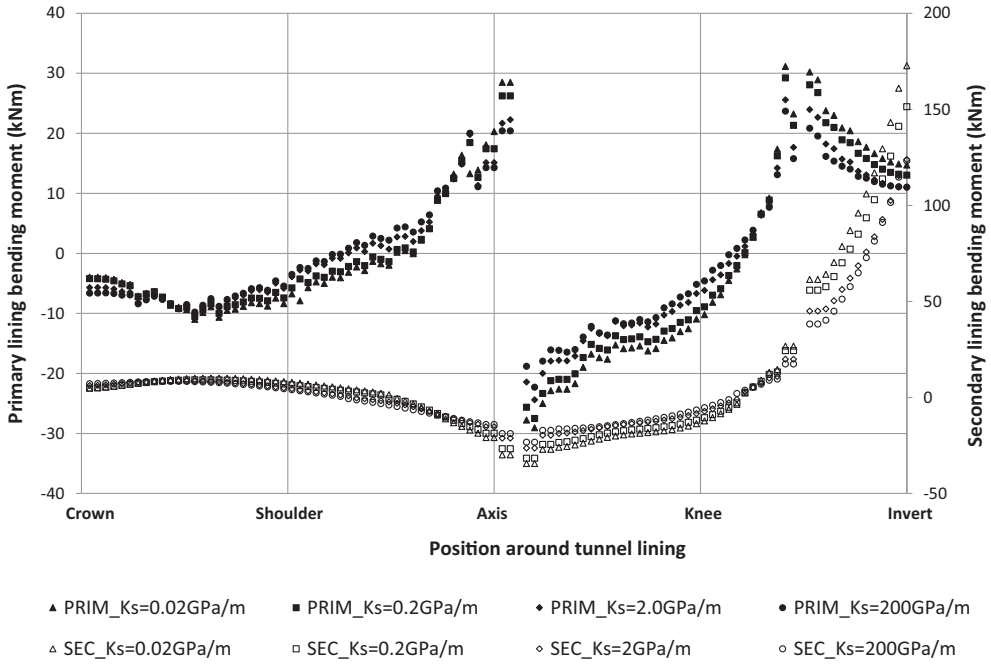

Fig. 23. Sensitivity of primary and secondary lining bending moment to shear interface stiffness Ks (Kn = 4GPa/m).

(Table 6) is also reducing as P/S increases. Hence, it is necessary to compare Fig. 26 with Table 6. From this, it is evident that first reinforcement is always required at the invert. Second, the crown also requires reinforcement for all cases except for $P/S = 6.0$. Finally, the remainder of the secondary lining, between the shoulder and the knee, is safe for all cases.

The sensitivity of the normal and shear interface stresses to $P/S \geq 1$ is shown in Figs. 27 and 28. The smaller the P/S ratio, the larger the normal interface stress, mainly due to the greater stiffness of the thicker secondary lining. The highest normal tension is approximately 170 kPa, at axis level (Fig. 27). In addition, the smaller the P/S ratio, the greater the shear interface stress (Fig. 28),

Please cite this article in press as: Bloodworth, A., & Su, J., Numerical analysis and capacity evaluation of composite sprayed concrete lined tunnels, Underground Space (2018), https://doi.org/10.1016/j.undsp.2017.12.001

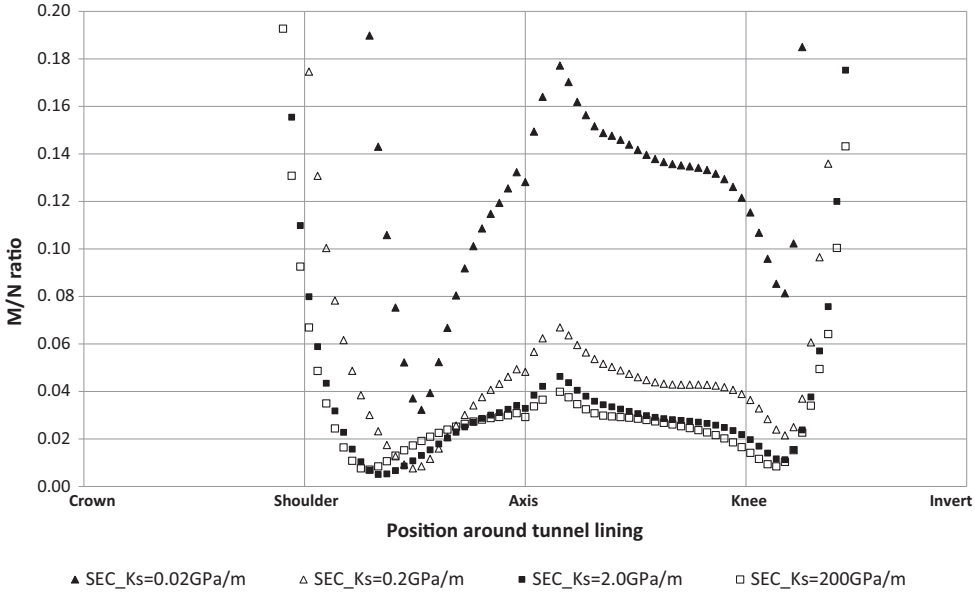

Fig. 24. Sensitivity of M/N ratios for secondary lining to shear interface stiffness Ks (Kn = 4GPa/m).

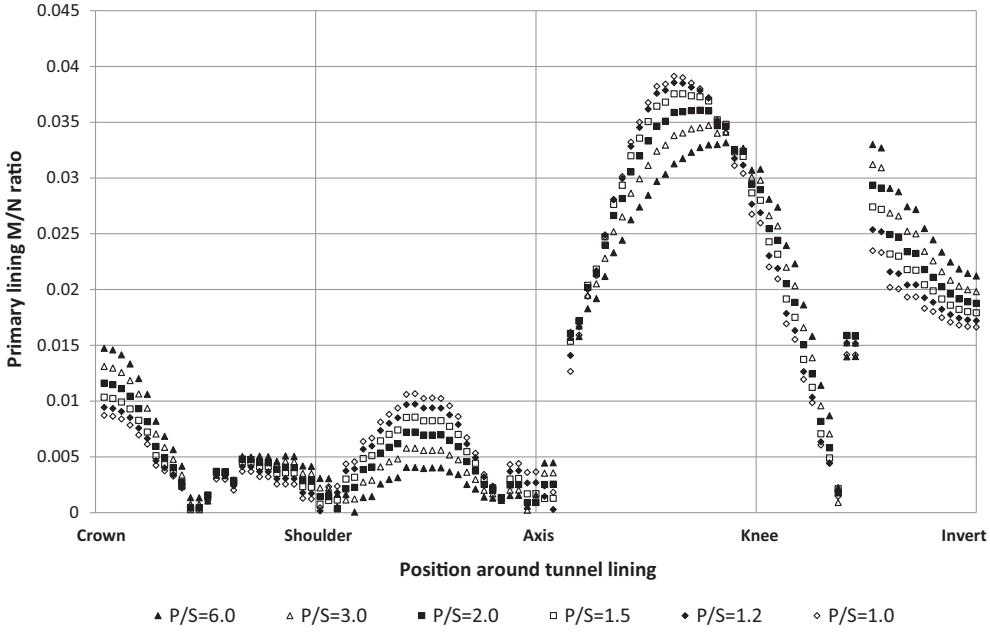

Fig. 25. Sensitivity of primary lining M/N ratio to varying primary/secondary lining thickness ratio P/S (Kn = 4GPa/m, Ks = 2 GPa/m).

confirming a finding during the model verification that the degree of composite action (i.e., the magnitude of shear interface stress) is greatest when the interface is at half depth of composite linings. All shear interface stresses are less than 170 kPa, which are well below the limit of 2 MPa.

Table 7 provides the lining efficiency for the six combinations of lining thickness investigated above. As S reduces, the lining efficiency improves significantly by approximately 40%, from 55.5 mm/m for $S = 300$ mm to 32.4 mm/m for $S = 50$ mm.

Analysis of adjacent construction

These analyses aim to check the robustness of the interface as bending is increased by inducing distortion in the lining. The possible sources of distortion include surcharge on the tunnel or anisotropic initial ground stresses. For this study, nearby construction causing stress relief either vertically or horizontally was considered. Such construction (e.g., tunneling or diaphragm walling) was not modeled explicitly but rather by hypothetical forces applied in the ground to introduce strains of representative magnitudes.

Please cite this article in press as: Bloodworth, A., & Su, J., Numerical analysis and capacity evaluation of composite sprayed concrete lined tunnels, Underground Space (2018), https://doi.org/10.1016/j.undsp.2017.12.001

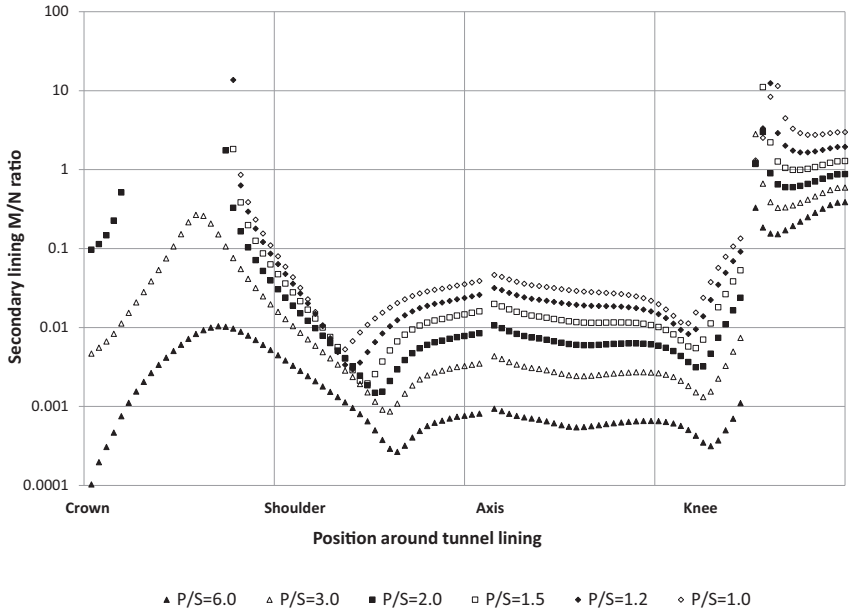

Fig. 26. Sensitivity of secondary lining M/N ratio to varying primary/secondary lining thickness ratio P/S (Kn = 4 GPa/m, Ks = 2 GPa/m).

Table 6
Safe ratios of M/N for secondary linings of different thicknesses.

P/S ratio	6.0	3.0	2.0	1.5	1.2	1.0
Secondary lining thickness (mm)	50	100	150	200	250	300
Safe M/N ratio	0.022	0.046	0.068	0.088	0.11	0.13

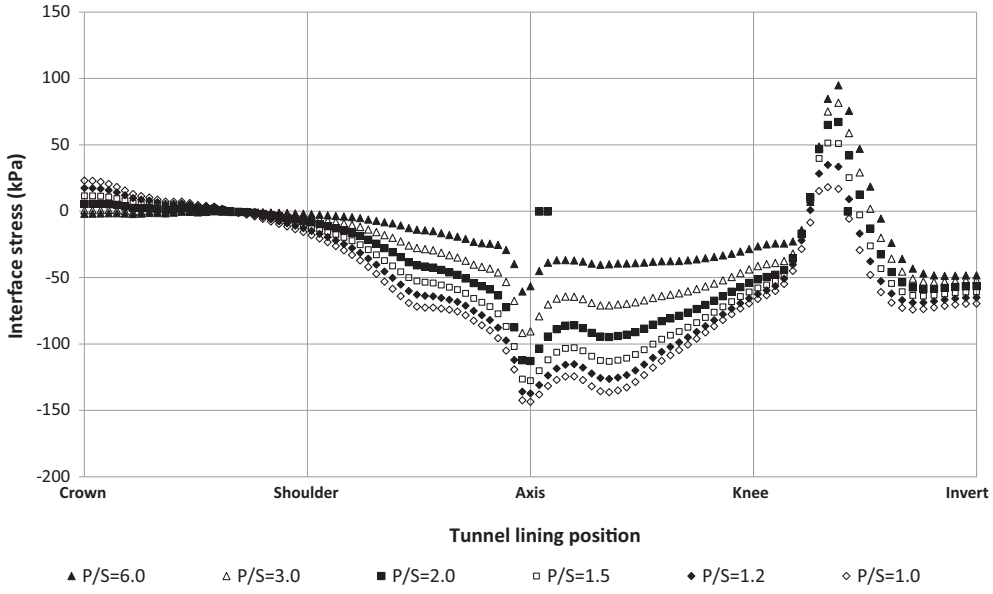

Fig. 27. Sensitivity of normal interface stress to varying primary/secondary lining thickness ratio (P/S ≥ 1) (Kn = 4 GPa/m, Ks = 2 GPa/m).

Atkinson and Salfors (1991) and Mair (1993) suggest that shear strains of 0.1–1% can occur due to tunneling. Hypothetical forces comprising 100 kPa pressure were applied at five different clear distances from the tunnel to the right or beneath (Fig. 29), generating a shear strain of roughly 1% in the ground approximately from the axis upward, with lower strains below the axis level because of the increase in ground stiffness with depth. Hence, the

Please cite this article in press as: Bloodworth, A., & Su, J., Numerical analysis and capacity evaluation of composite sprayed concrete lined tunnels, Underground Space (2018), https://doi.org/10.1016/j.undsp.2017.12.001

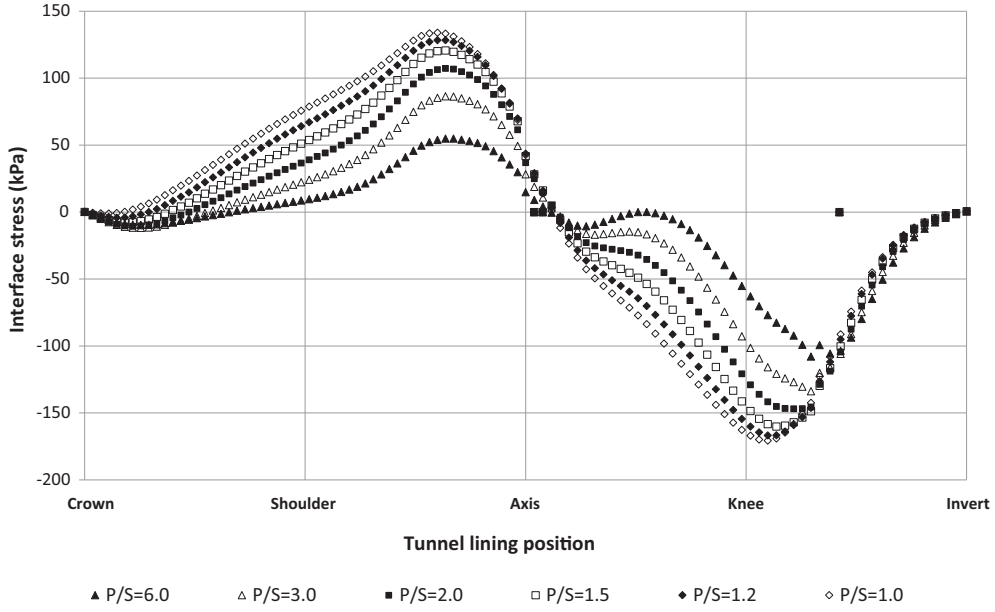

Fig. 28. Sensitivity of shear interface stress to varying primary/secondary lining thickness ratio (P/S ≥ 1) (Kn = 4 GPa/m, Ks = 2 GPa/m).

Table 7
Lining efficiency for varying secondary lining thickness.

Primary lining thickness (mm)	300					
Secondary lining thickness S (mm)	300	250	200	150	100	50
Total lining thickness $T = P + S$ (mm)	600	550	500	450	400	350
Tunnel external diameter D (m)	10.8					
Lining efficiency T/D (mm/m)	55.5	50.9	46.3	41.7	37.0	32.4

overall shear strains generated are toward the upper limit of the desired range. Base case interface stiffness values and 300 mm thick primary and secondary lining layers were used.

Proximity of the adjacent construction is expressed by the gap ratio R:

$$R = \frac{B}{D} \tag{2}$$

where B is the clear distance from tunnel extrados to the line of application of the hypothetical load and D is the tunnel diameter.

The key interest is the robustness of the CSL tunnel, i.e., not overstressing, and therefore, preventing damage to the interface and the potential to lose composite action. Therefore, only the interface stress results are presented as a function of R. The lining load effects are available in the Supplemental data (Figs. S15–S28).

Fig. 30 shows the normal interface stresses due to the construction at the right side of the tunnel. Maximum compression occurs at the connection between the knee and invert and maximum tension at the axis, both with a magnitude of 400 kPa, which is approximately 50% of the tensile stress limit found in element tests on "dry" specimens by Su and Bloodworth (2016). Fig. 31 shows that the maximum interface shear stress occurs between the axis and the knee, with a magnitude of approximately 650 kPa, which is significantly lower than the shear stress limit of 2 MPa.

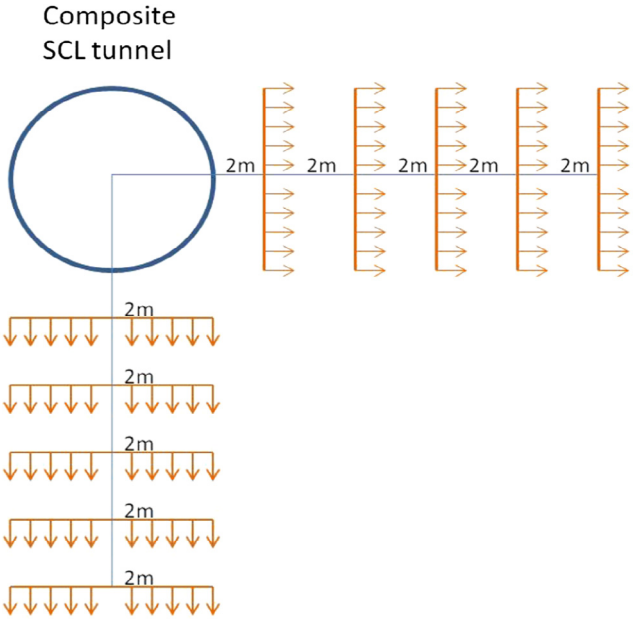

Fig. 29. Schematic of notional forces applied to CSL model to simulate nearby construction.

Please cite this article in press as: Bloodworth, A., & Su, J., Numerical analysis and capacity evaluation of composite sprayed concrete lined tunnels, Underground Space (2018), https://doi.org/10.1016/j.undsp.2017.12.001

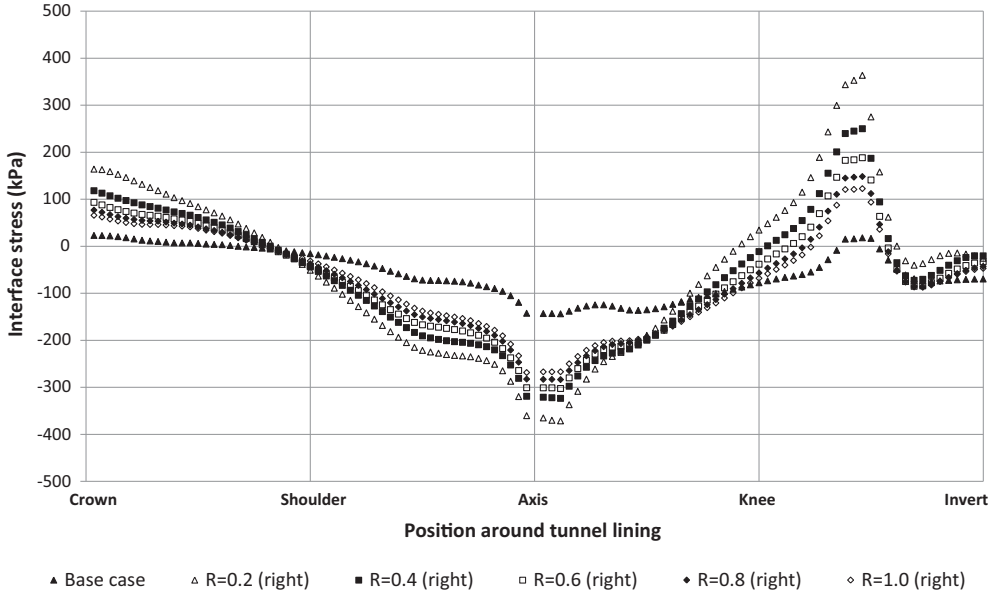

Fig. 30. Sensitivity of normal interface stress to right hand side construction at gap ratio R (Kn = 4 GPa/m, Ks = 2 GPa/m).

For construction beneath the tunnel, the smaller the value of *R*, the greater the change in the normal and shear interface stresses at all lining positions. However, all interface stresses are less than 50 kPa and therefore, are well within limits. Relevant plots are included in the Supplemental data (Figs. S15–S22).

Discussion of parametric studies

The parametric studies have examined the sensitivity of interface shear and normal stresses to interface shear and normal stiffness, primary/secondary lining thickness ratio, and effect of unequal loading on the tunnel. The starting point was a base case pair of interface stiffness values *Kn* = 4 GPa/m and *Ks* = 2 GPa/m obtained from long-term tests on "dry" samples. Comparison of stresses showed that they were within the minimum strengths obtained on the same "dry" specimens (0.8 MPa tensile and 2.0 MPa shear respectively). On no occasion were these strengths exceeded in the parametric study—the highest interface stresses observed were 160 kPa in tension and 220 kPa in shear (Figs. S2 and S3).

The effect of membrane saturation on the measured values of membrane strength and stiffness is known to be significant (Holter & Geving 2015). Holter (2015) reported ranges of shear strengths of 0.55–0.85 MPa, shear stiffness of 300–350 MPa/m, and tensile strengths of 0.35–1.0 MPa when the membrane was partially saturated by immersion in water (normal stiffness was not given). The highest interface stresses obtained here with base case *Kn* and *Ks* are

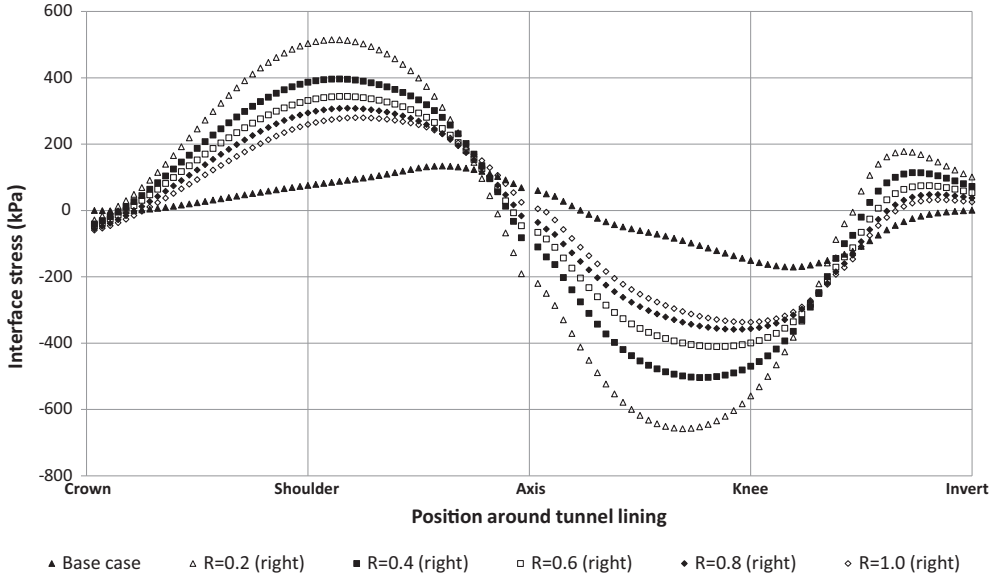

Fig. 31. Sensitivity of shear interface stress to right hand side construction at gap ratio R (Kn = 4 GPa/m, Ks = 2 GPa/m).

Please cite this article in press as: Bloodworth, A., & Su, J., Numerical analysis and capacity evaluation of composite sprayed concrete lined tunnels, Underground Space (2018), https://doi.org/10.1016/j.undsp.2017.12.001

150 kPa tensile and 170 kPa shear (Figs. 20 and 21), which are well below the test results by Holter (2015), with a minimum factor of safety of 2.3 for tension (0.35 MPa/0.15 MPa) and 3.2 for shear (0.55 MPa/0.17 MPa).

These factors of safety are obtained from analyses with typical "dry" membrane stiffness values. It is known from Holter (2015) that interface stiffness is reduced by membrane partial saturation. For example, the short-term value of shear stiffness of 0.35 GPa/m, implying a long-term value half of that (0.175 GPa) is approximately 10% of the "dry" base case *Ks*. The parametric study shows that for $Ks = 0.2$ GPa/m, the maximum tensile and shear interface stresses are 110 kPa and 70 kPa respectively, increasing the safety factor to 3.2 for tension (0.35 MPa/0.11 MPa) and 7.9 for shear (0.55 MPa/0.07 MPa). Interface shear stresses are known to reduce as *Ks* reduces and the same is true for normal stress (Fig. 20). Reducing the secondary lining thickness reduces further both the tension and shear interface stresses (Figs. 27 and 28). Both these effects should increase the factor of safety against membrane failure when partially saturated. Another point to note is that the test data of Holter (2015) were obtained when the membrane was immersed in water, which is probably an overestimation of realistic moisture boundary conditions.

Hence, overall, there can be confidence in composite action that would occur and be maintained even when the membrane is fully saturated. This assumes that first, the water pressure does not exceed the tensile strength of the interface, causing de-bonding (35 m head of water for the lowest strength reported by Holter, which is rarely exceeded in soft ground urban tunneling situations such as in London). Second, it was shown that high tensile interface stresses can be induced by unequal loading, such as adjacent construction at close proximity (which caused a tensile strength of 400 kPa that exceeds Holter's minimum observed strength of 350 kPa). It would therefore be prudent to impose an exclusion zone for nearby construction until further research on the realistic degree of membrane saturation in a CSL tunnel in soft ground conditions can be carried out and expected resulting membrane bond strengths can be obtained.

Conclusions

Numerical analysis has been carried out on a composite shell lined tunnel typical of a metro station platform or concourse tunnel in soft ground of low permeability (such as the London basin). Ground behavior is considered undrained in the short term when only the primary lining is loaded, and drained in the long term with consolidation loading and water pressure shared between the primary and secondary linings. Base case interface stiffness values were obtained from laboratory tests on lining elements with "dry" ethyl-vinyl-acetate spray-applied membrane, and then varied in a parametric study encompassing the range of practical workmanship variation as well as "wet" membrane conditions. Although the analyses have been carried out for a specific geometry, ground conditions, and range of interface parameters, the fundamental behavior observed and trends in the results obtained should nevertheless be informative for designers of other tunnels, who should undertake their own analyses using interface properties that are appropriate for their own project.

The analyses show the tunnel to demonstrate a reasonable degree of composite action, which may be high enough to induce large bending moments in the secondary lining, requiring additional reinforcement in its crown. It is therefore not conservative to design a CSL tunnel simply as a double shell, without considering the interface shear stiffness. The real benefit of CSL tunnels is that interface tensile and shear bonds prevent long-term water pressure from applying only to the secondary lining; instead, it acts mostly on the primary lining. This leads to the possibility of reducing the secondary lining thickness to improve the overall lining efficiency, while making both primary and secondary linings structurally safer, with the secondary less likely to require reinforcement. Interface compressive, tensile, and shear stress limits observed in previous element tests on "dry" samples are sufficient to resist interface stresses occurring in the parametric studies on interface stiffness and secondary lining thickness, and even when the known effect of membrane partial saturation on interface strength and stiffness is taken into account, composite action is still expected to be maintained. The margin of safety against tensile membrane de-bonding was only found to be inadequate under a case of unequal loading induced by construction in close proximity to the tunnel. It would be prudent to take precautions in such cases (for example, to impose an exclusion zone for nearby construction) to ensure a sufficient factor of safety. This is until further research on the realistic degree of membrane saturation in a CSL tunnel in soft ground conditions can be carried out and expected resulting membrane bond strengths are obtained.

Acknowledgments

The authors gratefully acknowledge the financial support of Mott MacDonald and Normet in carrying out this study.

Appendix A. Supplementary material

Supplementary data associated with this article can be found, in the online version, at https://doi.org/10.1016/j.undsp.2017.12.001.

References

Atkinson, J. H., & Salfors, G. (1991). Experimental determination of soil properties. General Report to Session 1. In *Proc. 10th Euro. conf. soil mechanics and foundation engng*. (pp. 915–956). Rotterdam: Balkema.

Betonverein, Osterreichischer. (1999). *Sprayed concrete guideline—Application and testing*. Vienna: Austrian Tunnelling Society.

BSI (1992). *Design of concrete structures — Part 1-1: General rules and rules for buildings*. London: British Standards Institution.

Chang, Y., & Stille, H. (1993). Influence of early age properties of sprayed concrete to tunnel construction sequence. In *Proc. sprayed concrete for underground support VI* (pp. 110–117). Reston: American Society of Civil Engineers.

Chang, J., Scott, J. M., & Pound, C. (2001). Numerical study of Heathrow cofferdam. In *Proc. 2nd int. sympos. FLAC and numerical modelling in geomechanics* (pp. 163–169). Balkema.

Clayton, C. R. I., Hope, V. S., Heymann, G., Van der Berg, J. P., & Bica, A. V. D. (2000). Instrumentation for monitoring sprayed concrete lined soft ground tunnels. *Proceedings of the Institution of Civil Engineers-Geotechnical Engineering, 143*(3), 119–130.

Clayton, C. R. I., Van Der Berg, J. P., Heymann, G., Bica, A. V. D., & Hope, V. S. (2002). The performance of pressure cells for sprayed concrete tunnel linings. *Géotechnique, 52*(2), 107–115.

Clayton, C. R. I., Van Der Berg, J. P., & Thomas, A. H. (2006). Monitoring and displacements at Heathrow Express Terminal 4 station tunnels. *Géotechnique, 56*(5), 323–334.

De Battista, N., Elshafie, M., Soga, K., Williamson, M., Hazelden, G. & Hsu, Y.S. (2015). Strain monitoring using embedded distributed fibre optic sensors in a sprayed concrete tunnel lining during the excavation of cross-passage. In *Proc. 7th Int. conf. on structural health monitoring of intelligent infrastructure*. Winnipeg: Int. Society for Structural Health Monitoring of Intelligent Infrastructure.

Dimmock, R., & Lackner, J. (1998). NATM on JLE 102. *Concrete Engineering International*, 15–22.

Eadington, J., & O'Brien, T. (2011). Stiffness parameters for a deep tunnel – Developing a robust parameter selection framework. In *Proc. 15th Euro. conf. on soil mechanics and geotechnical engng*. Athens: Hellenic Society for Soil Mechanics and Geotechnical Engineering.

Hasik, O., Junek, J., & Zamecnik, M. (2015). Metro Prague – use of sprayed waterproofing membrane in deep level station. In *Proc. ITA World Tunnel Congress 2015*. Zagreb: HUBUTGM.

Holter, K. G. (2016). Performance of EVA-based membranes for SCL in hard rock. *Rock Mechanics and Rock Engineering, 49*(4), 1329–1358.

Holter, K. G., Bridge, R., & Tappy, O. (2010). Design and construction of permanent waterproof tunnel linings based on sprayed concrete and spray-applied double-bonded membrane. In *Proc., 11th int. conf. underground construction Prague* (pp. 121–126). Prague: Czech Tunnelling Association.

Holter, K. G., & Geving, S. (2015). Moisture transport through sprayed concrete tunnel linings. *Rock Mechanics and Rock Engineering, 49*(1), 243–272.

Hurt, J. (2002). Primary ways to save – Harding prize paper. *Tunnels and Tunnelling International, 2*, 44–45.

Itasca (2008). *FLAC version 6.0 Fast Lagrangian Analysis of Continua, Theory and Background, User Manual*. Minneapolis: Itasca Consulting Group Inc.

Jager, J. (2016). Structural Design of Composite Shell Linings. In *Proc. World Tunnel Congress 2016*. Society for Mining, Metallurgy, and Exploration.

Johnson, R. P., Swallow, F. E., & Psomas, S. (2016). Structural properties and durability of a sprayed waterproofing membrane for tunnels. *Tunnelling and Underground Space Technology, 60*, 41–48.

Jones, B., Thomas, A. H., Hsu, Y. S., & Hilar, M. (2008). Evaluation of innovative sprayed-concrete-lined tunnelling. *Proceedings of the Institution of Civil Engineers-Geotechnical Engineering, 161*(3), 137–149.

Mair, R. J. (1993). Developments in geotechnical engineering research: applications to tunnels and deep excavations. *Proceedings of the Institution of Civil Engineers-Geotechnical Engineering- Civil Engineering, 3*, 27–41.

Marcher, T., John, M., & Ristic, M. (2011). Determination of load-sharing effects in sprayed concrete tunnel linings. In *Proc. underground construction 2011*. London: British Tunnelling Society.

Mašín, D. (2009). 3D modeling of an NATM tunnel in high K_0 clay using two different constitutive models. *Journal of Geotechnical and Geoenvironmental Engineering, 135*(9), 1326–1335.

Morgan, T., Wolstenholme, A., & Dulake, C. (2013). Crossrail tunnelling on an epic scale. *Ingenia, 56*, 14–21.

Nakashima, M., Hammer, A. L., Thewes, M., Elshafie, M., & Soga, K. (2015). Mechanical behaviour of a sprayed concrete lining isolated by a sprayed waterproofing membrane. *Tunnelling and Underground Space Technology, 47*, 143–152.

Nermoen, B., Grøv, E., Holter, K.G. & Vassenden, S. (2011). Permanent waterproof tunnel lining based on sprayed concrete and spray-applied double-bonded membrane. First Norwegian experiences with testing under freezing conditions, design and construction. In: *Proceedings of 6th international symposium on sprayed concrete*. Tromso, Norway.

O'Brien, A., & Harris, D. (2013). Geotechnical characterisation, recent development and applications. In *Proc. 12th Int. conf. underground construction*. Prague: Czech Tunnelling Society.

Panet, M. & Guenot, A. (1982). Analysis of convergence behind the face of a tunnel. In *Proc. tunnelling 82 (pp. 197–204)*. London: Institution of Mining and Metallurgy.

Pickett, A. (2015). Crossrail sprayed concrete linings design. In M. Black, C. Dodge, & U. Lawrence (Eds.). *Crossrail project: Infrastructure design and construction* (vol. 1, pp. 137–153). London: ICE Publishing.

Pillai, A., Jung, H., Clement, F., Wilson, C. & Traldi, D. (2017). Sprayed concrete composite tunnel lining – load sharing between the primary and secondary lining, and its benefit in reducing the structural thickness of the lining, In: *Proc. world tunnel congress 2017*. Sandvika, Norway: Norwegian Tunnelling Society.

Powell, D. B., Sigl, O., & Beveridge, J. P. (1997). Heathrow Express – design and performance of platform tunnels at Terminal 4. In *Proc. Tunnelling 97* (pp. 565–593). London: Institution of Mining and Metallurgy.

Sauer, G., Gall, V., Bauer, E. & Dietmaier, P. (1994). Design of tunnel concrete linings using limit capacity curves. In *Proc. 8th int. conf. on computer methods and advances in geomechanics* (pp. 2621–2626). Rotterdam: Balkema.

Scott, J. M., Pound, C., & Shanghavi, H. B. (2003). Heathrow airside road tunnel: wall design and observed performance. In *Proc. int. conf. underground construction* (pp. 281–292). London: British Tunnelling Society.

Su, J. (2015). Laboratory element tests and numerical modelling to investigate the performance of composite sprayed concrete lined tunnels in soft ground. *PhD Thesis*, University of Southampton.

Su, J., & Bloodworth, A. (2016). Interface parameters of composite sprayed concrete linings in soft ground with spray-applied waterproofing. *Tunnelling and Underground Space Technology, 59*, 170–182.

Su, J., & Thomas, A. (2015). Design of sprayed concrete linings in soft ground—a Crossrail perspective. In M. Black, C. Dodge, & U. Lawrence (Eds.). *Crossrail Project: Infrastructure design and construction* (vol. 1, pp. 123–136). London: ICE Publishing.

Sun, Y., McRae, M., & Van Greunen, J. (2013). Load sharing in two-pass lining systems for NATM tunnels. In *Proc. rapid excavation and tunnelling conference* (pp. 1178–1191). Society for Mining, Metallurgy, and Exploration.

Thomas, A. H. (2004). Numerical modelling of sprayed concrete lined (SCL) tunnels. PhD Thesis, University of Southampton.

Thomas, A. H., & Pickett, A. P. (2011). The design of composite sprayed linings. In *Proc. 6th int. symposium on sprayed concrete*. Tromso: Norwegian Concrete Association.

Vogel, F., Sovják, R. & Pešková, Š. (2017). Static response of double shell concrete lining with a spray-applied waterproofing membrane. *Tunnelling and Underground Space Technology*, 68, 106–112.

Zeidler, K., & Gall, V. (1997). London Bridge Station, Jubilee Line extension. In *Proc. rapid excavation and tunnelling conference* (pp. 631–654). Society for Mining, Metallurgy and Exploration.

Please cite this article in press as: Bloodworth, A., & Su, J., Numerical analysis and capacity evaluation of composite sprayed concrete lined tunnels, Underground Space (2018), https://doi.org/10.1016/j.undsp.2017.12.001